# Chapter 10
# Electrochemical Promotional Role of Under-Rib Convection-Based Flow-Field in Polymer Electrolyte Membrane Fuel Cells

**Hyung-Man Kim and Vinh Duy Nguyen**

**Abstract** Literature data on the promotional role of under-rib convection for polymer electrolyte membrane fuel cells (PEMFCs) fueled by hydrogen and methanol are structured and analyzed, with the aim of providing a guide to improve fuel cell performance through the optimization of flow-field interaction. Data are presented for both physical and electrochemical performance showing reactant mass transport, electrochemical reaction, water behavior, and power density enhanced by under-rib convection. Performance improvement studies ranging from single cell to stack are presented for measuring the performance of real operating conditions and large-scale setups. The flow-field optimization techniques by under-rib convection are derived from the collected data over a wide range of experiments and modeling studies with a variety of components including both single cell and stack arrangements. Numerical models for PEMFCs are presented with an emphasis on mass transfer and electrochemical reaction inside the fuel cell. The models are primarily used here as a tool in the parametric analysis of significant design features and to permit the design of the experiment. Enhanced flow-field design that utilizes the promotional role of under-rib convection can contribute to commercializing PEMFCs.

**Keywords** Electrochemical reaction · Electrochemistry · Exchange interactions · Flow-field design · Fuel cell performance · Mass transfer · Polymer electrolyte membrane fuel cell · Under-rib convection · Water management

H.-M. Kim (✉) · V.D. Nguyen
Department of Mechanical Engineering and High Safety Vehicle Core Technology Research Center, INJE University, 607 Eobang-Dong, Gimhae-Si, Gyongsangnam-Do 621-749, Republic of Korea
e-mail: mechkhm@inje.ac.kr



Inamuddin et al. (eds.), *Organic–Inorganic Composite Polymer Electrolyte Membranes*, DOI 10.1007/978-3-319-52739-0_10

## Nomenclatures

| | |
|---|---|
| $\Delta p_{\text{tot}}$ | Total pressure drop |
| $z_{\max}$ | Total length of the path |
| $K_{\text{ch}}$ | Channel permeability derived from the Hagen–Poiseuille equation |
| $\Delta c_{\text{tot}}$ | Total concentration loss |
| $q_{\text{rib}}$ | Under-rib convection flowrate |
| $K_{\text{gdl}}$ | Flow permeability of the GDL |
| $\overline{\dot{v}}_{\text{spec}}$ | Mean specific volume flow |
| $\dot{V}$ | Inlet volume flow |
| $\dot{V}_{\text{local}}^{\text{meander}}$ | Integral of the local volume flow (l/h) |
| $\overline{\dot{v}}_{\text{spec}}^{\text{meander}}$ | Specific volume flow in the meander channel |
| $\overline{\dot{v}}_{\text{spec}}^{\text{diff}}$ | Total specific flow through the diffusion layer |
| $P_{\text{cell}}$ | Cell output power density |
| $W_P$ | Pressure drop loss |
| AFC | Alkaline fuel cell |
| BOP | Balance of plant |
| CFD | Computational fluid dynamic |
| CL | Catalyst layer |
| DMFC | Direct methanol fuel cell |
| EIS | Electrochemical impedance spectroscopy |
| GDL | Gas diffusion layer |
| GFF | Grid flow-field |
| MCFC | Molten carbonate fuel cell |
| MEA | Membrane electrolyte assembly |
| MFF | Original design mixed parallel and serpentine |
| MPL | Microporous gas diffusion layer |
| MSFF | Multi-serpentine |
| OCV | Open-circuit voltages, $E_0$ |
| ORR | Oxygen reduction reaction |
| PAFC | Phosphoric acid fuel cell |
| PEMFC | Polymer electrolyte membrane fuel cell |
| PFF | Parallel flow-field |
| PTFE | Polytetrafluoroethylene |
| SFF | Single serpentine |
| SSFF | Single serpentine flow-field |
| SOFC | Solid oxide fuel cell |
| VOF | Volume of fluid |
| $q_{\text{tot}}$ | Total flow rate |

## 1 Introduction

Fuel cells generate fewer harmful emissions and are more efficient compared with the Carnot efficiency of heat engines, because of converting the chemical energy of fuels directly into electricity without combustion [1]. Polymer electrolyte membrane fuel cells (PEMFCs) were first employed in the Gemini space program in the early 1960s. Fuel cells are expected to play a significant role in the strategy to produce positive global change, increase fuel efficiency, and decrease dependency on traditional fossil fuels. Fuel cells and direct electrochemical fuels, particularly hydrogen, provide the promise of being one of the several possible long-term solutions to the improvement of energy efficiency, energy sustainability, energy security, and the reduction of greenhouse gases. Significant environmental benefits are expected for fuel cells, particularly in the area of energy conversion for electric power generation and transportation. There are five types of fuel cells, which are differentiated on the basis of their electrolytes: (i) the polymer electrolyte membrane fuel cell (PEMFC), (ii) the phosphoric acid fuel cell (PAFC), (iii) the alkaline fuel cell (AFC), (iv) the molten carbonate fuel cell (MCFC), and (v) the solid oxide fuel cell (SOFC). While all five fuel cell types are based on the same underlying electrochemical principles, they operate at different temperature regimens, incorporate different materials, and often differ in their fuel tolerance and performance characteristics [2].

The hydrogen-fed proton exchange membrane fuel cells and liquid methanol-fed direct methanol fuel cells (DMFCs) using Nafion®-based polymer electrolyte membranes operate at low temperature (typically less than 100 °C). These low-temperature operating fuel cells are well suited for transportation, portable, and micro-fuel cell applications because of the requirement of fast start-up and dynamic operation in those applications. Some of the sulfonated hydrocarbon polymer membranes show high proton conductivity for potential operation at 100–120 °C [3]. The cathodes in DMFCs fueled by methanol, are similar to the cathodes of PEMFCs fueled by hydrogen; However, anode catalysts in DMFCs are typically high-loading Pt/Ru on high-surface blacks and are used at higher electrode loadings than those of PEMFCs [4]. The basic processes of both PEMFCs and DMFCs are shown in Fig. 1. In addition to the effects of electrochemical oxidation and reduction processes, the performance of the DMFC is affected by methanol permeation from the anode to the cathode, where the methanol is chemically oxidized. Although PEMFCs and DMFCs have similar theoretical open-circuit voltages, $E_0$, of 1.229 and 1.214 V, respectively, the methanol permeation that occurs during the process lowers the DMFC cell voltage by several hundreds of mV [5].

Technical progress in the design and manufacture of PEMFCs has been dramatic in recent years. In the 1970s, a chemically stable cation-exchange membrane, Nafion®, based on sulfonated polytetrafluoroethylene, was developed by Dupont which led to its large-scale use in the chlor-alkali production industry, energy storage, and fuel cells. During the past two decades, research on the development of PEMFCs with a Nafion® membrane as the electrolyte have received much attention.

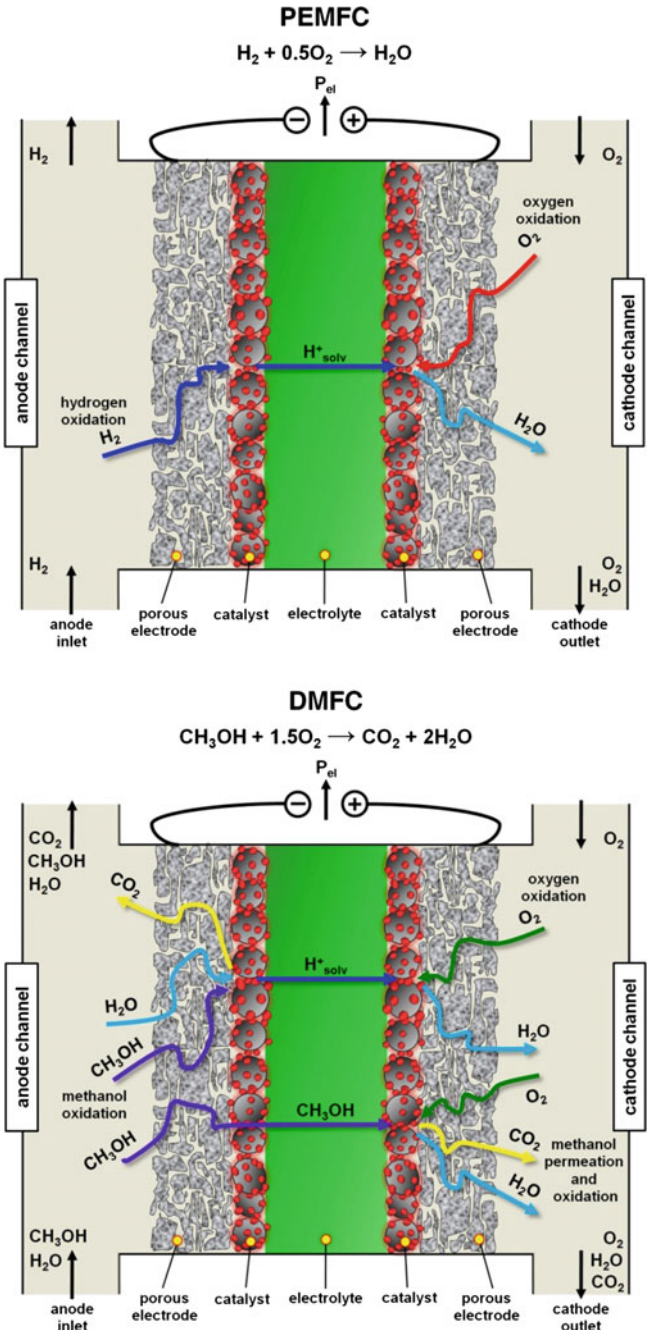


**Fig. 1** Principles of PEMFC and DMFC with proton exchange membranes. *Source* Ref. [5]

However, PEMFCs will need to be competitive with the established and highly developed internal combustion engine and other forms of power generation on an economic and consumer basis. Although much progress has been made in the development of the PEMFC, significant technical challenges still remain in a number of areas including reliability, durability, cost, operational flexibility, simplification, and integration of the underlying technology, fundamental understanding, and life cycle impact. To close technological gaps fundamental understanding, new advanced materials and associated engineering design and modeling are required. Many researchers have therefore recently focused on single cells of PEMFC and their components that involve novel membrane electrolytes, catalysts, and structure, electrochemical reaction mechanisms and kinetics, as well as electrode materials and preparation [6].

For a given membrane electrode assembly (MEA), the power density of a fuel cell stack can be significantly increased by reducing the profile of the bipolar plates. Bipolar plate design as a whole and flow channel layout configuration in particular are potential areas of research to make this alternative clean power source compatible to its counterparts. As one step forward, the interdigitated flow-field, in which baffles are added at the ends of some channels, was proposed. The baffle design forces the reactants to flow through the gas diffusion layer (GDL), and the actual force of this reactant flow helps blow out the liquid water trapped in the inner layers of the electrodes. With the interdigitated flow-field design, the mass transport rates of the reactants from the flow channel to the inner catalyst layer were improved, and the water flooding problem at the cathode was significantly reduced [7]. An increase of as much as 50% in the output power density was achieved by appropriate distribution of the gas flow-field alone [8]. Other more complex flow-field patterns and designs that combine more than one of the common patterns have also been reported, particularly for larger MEAs.

In early studies on flow-field development, cross convection has been widely ignored. In two of the first few studies to address this effect, two borderline cases for a serpentine design were distinguished: one in which all the fluid follows through the channel and one in which all the fluid passes through the GDL. The latter reduces the pressure drop over the flow-field. The authors concluded that, for GDLs with high permeability, it is important to keep the pressure drop along the channel low to reduce the risk of unequal reactant distribution due to dominant cross convection [5]. Recently, a number of researchers [9–42] have experimentally and numerically shown that convection in the porous diffusion layer affects transportation of mass and heat, liquid water removal and pressure drop, in PEMFCs. The convection transport mechanism has been referred to as gas–liquid two-phase flow [9], convection through the GDL [14], channel-to-channel gas crossover or cross convection [15–18], cross-leakage flow [21], and sub- or under-rib convection [27–38]. In this paper, we hereafter refer to this particular transport mechanism as ‘under-rib convection.’ Under-rib convection has recently been recognized as a non-negligible transport process that influences the performance of PEMFCs and DMFCs as a result of the higher GDL permeability that it produces.

The aim of this study is to provide a guide to the promotional role of under-rib convection in PEMFCs that covers a wide spectrum of the relevant scientific, engineering, and technical aspects of this phenomenon within the highly interdisciplinary nature of the fuel cell field. To achieve this, a large body of under-rib convection related data were screened and structured. Our motivations for undertaking the literature review of a particular aspect of PEMFC flow-field design are manifold. First, an analysis of the literature shows that under-rib convection between neighboring channels feeds reactants through GDL to the catalyst layer for mass transport and electrochemical reaction and enables more effective utilization of electrocatalysts by increasing reactant concentrations. Second, a number of particular aspects of PEMFC performance, such as liquid water removal, uniformity of concentration, pressure, temperature and current density, and output power, are promoted by under-rib convection, and these parameters have been screened and structured empirically through experimental and numerical studies. Finally, this work is intended to provide a basis for the optimization of flow-fields in which higher power density is achieved using the promotional role of under-rib convection; this optimization includes state-of-the-art designs that are likely to change as this technology continues to develop.

## 2 General Description of Performance Improvements in PEMFCs

Before presenting a review of the promotional role of under-rib convection, a brief analysis of recent progress in PEMFC design is presented that includes information on new advanced materials and their associated engineering design and modeling. Extensive surveys of the reliability, durability, cost, operational flexibility, technology simplification and integration, fundamental understanding, and life cycle impact of PEMFCs are already available [43–64]. As discussed later in this study, the analysis undertaken here nevertheless provides a better understanding of the PEMFC based on the collected literature data. The challenges that must be faced in application and commercialization of PEMFCs are emphasized. These challenges include continuous massive advancements in fundamental science and engineering research and in the technological development of PEMFCs.

The main components of a PEMFC power source are illustrated in Fig. 2. The PEMFC consists of (i) a single cell containing porous gas diffusion electrodes, a proton exchange membrane, catalyst layers, and current collectors with the reactant flow-fields (ii) a stack of cells in series with the current collectors, also serving as the bipolar plates, (iii) cell stacks connected in series or in parallel depending on the voltage and current requirements for specific applications, and (iv) the necessary auxiliaries for thermal and water management as well as for the compression of the gases. The unique feature of the PEMFC compared with the other types of fuel cells is that it has a solid proton-conducting electrolyte.

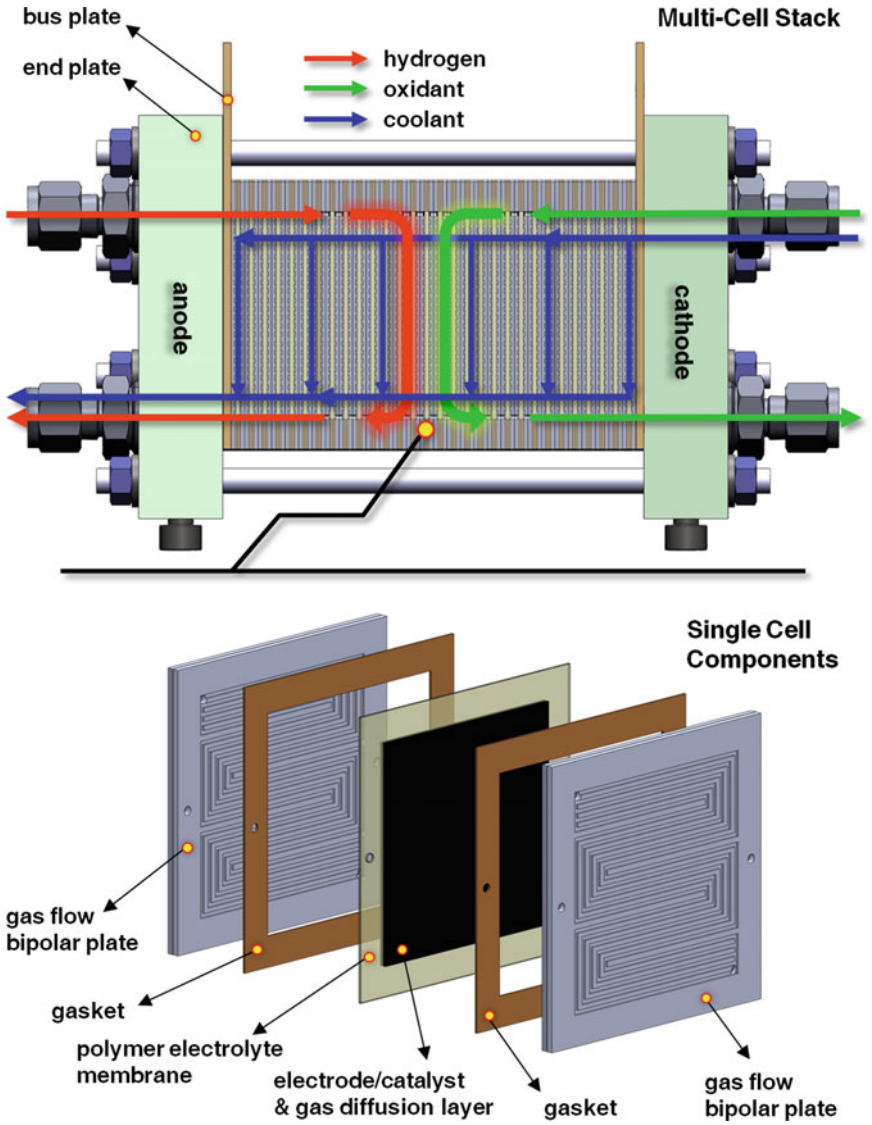


**Fig. 2** Schematic of PEMFC single cell components and multi-cell stack

PEMFCs generate a specific power (W/kg) and power density (W/cm$^2$) higher than any other type of fuel cell [43].

The development of new components with improved characteristics for fuel cell applications requires quantitative determination of their electrochemical performance under relevant fuel cell conditions. The most straightforward approach to this is to construct an MEA and measure the cell parameters in a single cell

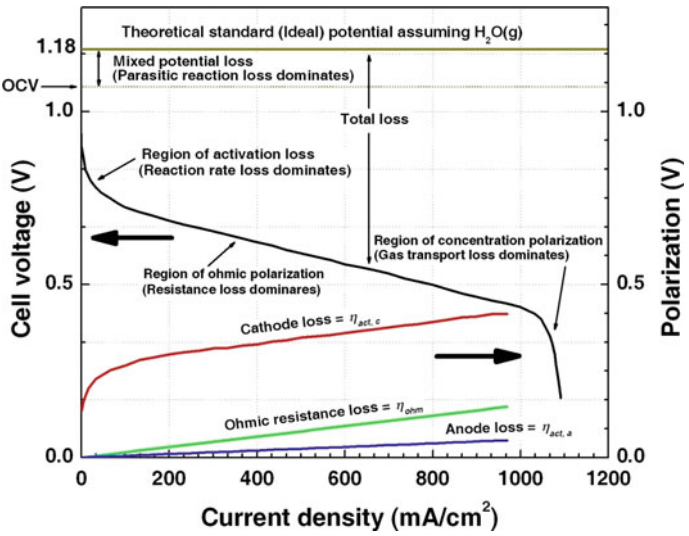


**Fig. 3** A typical curve of PEM fuel cell performance. *Source* Ref. [18]

configuration. A membrane electrode assembly includes an anode, a cathode, a membrane disposed between the anode and the cathode, and an extended catalyst layer between the membrane and the electrodes. Apart from the operation conditions, the conversion efficiency of a given MEA depends on several factors, including the type and thickness of both the membrane and the gas diffusion material, the nature of the binder used in the electrodes, and the binder-to-catalyst ratio. Single cell testing is relatively straightforward, and operation conditions can be accurately monitored because it allows specific control over humidity, reactant flow, and temperature. In addition, the ability to collect data from an operating electrochemical system can be alluring. Cell performance is often described by the polarization curve, i.e., cell voltage versus current density. A typical curve is shown in Fig. 3 [41]. In general, three main polarization losses can be identified: (i) activation losses, arising from charge transfer and other reaction kinetics; (ii) ohmic resistances, arising from the electrical resistances of the cell materials and interfaces, and (iii) mass transport limitations, arising from the limitations of mass transport. At low current densities, the shape of the curve is primarily determined by activation polarization; which gives the curve its characteristic logarithmic shape. Activation polarization plays an important role in cell performance because of the reaction rate on the electrode surface is restricted by sluggish electrode kinetics. Like a chemical reaction, the electrochemical reaction must overcome an activation barrier. This barrier usually depends on the electrode material. When pure hydrogen is used as fuel, the activation losses at the anode are negligible because the rate of the hydrogen oxidation reaction is much higher than the rate of the cathode reaction. Hence, the main source of activation overpotential is the cathode, at which oxygen reduction occurs. When current density increases,

the shape of the curve becomes approximately linear, reflecting the effect of ohmic losses. This is caused by both the resistance due to the migration of ions within the electrolyte and by the resistance due to the flow of electrons. It can be expressed by the product of cell current and the overall cell resistance. When current density is increased further, the curve begins to bend down due to mass transport overpotentials, which result from limitations in the availability of reactants at the catalyst surfaces. The main source of losses is again the cathode side because the diffusivity of oxygen is significantly lower than that of hydrogen due to the larger molecular size of oxygen [60].

Fuel cell efficiency, on the other hand, is directly proportional to the power density, which can be linked directly to the chemistry of the polymer membrane. Higher achievable power density directly translates to smaller, thus less expensive, fuel cells. A swift comparison of the obtained data those obtained with unmodified membranes is expected to provide useful information about the influence of the inorganic phase on the nanocomposite efficiency. Their effectiveness as a catalyst binder may be evident from an investigation of the interfacial effects of membranes on electrodes and catalysts. In the case of Class I membranes intended for high temperature operations, the methanol crossover flux versus methanol feed concentration can be collected, and the suitability of the membrane for DMFC applications may be determined from these data. The time stability of the membranes under different operating conditions may also be studied. Single cell testing will be of great advantage in fine-tuning hybrid membrane properties in order to give them commercial viability [64]. Henceforth, a major technical challenge is up-scaling single cell performance to stacks.

## *2.1 Proton Exchange Membrane*

The proton exchange membrane (PEM) is the vital component of a PEMFC that encourages fuel cell to attain high power densities. The role of the membrane between the electrodes is to conduct protons produced by the electrochemical reaction from the anode to the cathode. In the 1970s, DuPont developed a perfluorosulfonic acid membrane, Nafion®, which not only showed a twofold increase in specific conductivity but also extended the lifetime of the cell by four orders of magnitude [43]. Perfluorosulfonic acid membranes soon became a standard for PEMFC that remain continued till today. The Nafion® membrane consists of a copolymer of 3, 6-dioxo-4, 6-octane sulfonic acid with polytetrafluorethylene; the Teflon backbone of this structure creates the hydrophobic nature of the membrane, and hydrophilic sulfonic acid groups $\left(HSO_3^-\right)$ have been grafted chemically onto the backbone structure. The hydrophilic sulfonic acid groups cause the absorption of a large amount of water by the polymer, leading to hydration of the polymer [60]. The level of hydration and membrane thickness are two important factors that affect the performance of proton exchange membranes; both play important roles in the suitability of membranes for application in fuel cells.

PEMFC performance, which depends on the proton conductivity, also depends on the degree of humidity of the membrane. Higher proton conductivity is achieved at higher membrane humidity. One way to avoid water drag or water crossover is to reduce the membrane thickness, thereby enabling an improvement in fuel cell performance. Other advantages of reduced thickness include lower membrane resistance, cost effectiveness, and rapid hydration. However, because of the difficulties with durability and fuel bypass, there is a limit to the extent to which membrane thickness can be reduced. To achieve high efficiency in fuel cell applications, the polymer electrolyte membrane must possess the following desirable properties: high proton conductivity to support high currents with minimal resistive losses, zero electronic conductivity, adequate mechanical strength and stability, chemical and electrochemical stability under operating conditions, control of moisture in the stack, extremely low fuel or oxygen bypass to maximize columbic efficiency and production costs compatible with the intended application [53]. The Dow Chemical and Asahi Chemical Companies have synthesized advanced perfluorosulfonic acid membranes with shorter side chains and a higher ratio of $SO_3H$ to $CF_2$ groups. Compared to Nafion®, the lower equivalent weights of these membranes account for their higher specific conductivities and result in significant improvements in the PEMFC performance, i.e., approximately 50–100 mV increase in cell potential at 1 A/cm$^2$ over the Nafion® 115, which has approximately the same thickness ($\sim$100 μm) [66].

Proton exchange membrane is the key component of fuel cell systems that limit the lifetime of PEMFCs. Thus, the enhancement of the durability of PEMs is critical to the commercial viability of PEMFCs. In the past decade, membrane degradation mechanism studies have become a focus of attention. In recently published reports, membrane degradation is primarily classified as either chemical/electrochemical or physical. With respect to the former, hydrogen peroxide generated during fuel cell operation and its decomposition intermediate products, both of which have strong oxidative characteristics, have been considered one of the important factors resulting in membrane degradation. The formation of $H_2O_2$ was confirmed using a microelectrode in an operating fuel cell [67]. It was detected in the outlet stream of a cell with a Nafion® membrane [68]. Membrane durability was subsequently evaluated by both an ex situ Fenton test [69] and an in situ OCV accelerated test [70].

One of the major issues to be addressed in the development of proton-conducting nanocomposite and hybrid membranes for fuel cell applications is their high temperature stability since low temperature mitigates degradation [71]. Although fuel cell performance degradation was considerable under conditions in which the MEA was allowed to lose much water, no lowering of the open-circuit potential was observed, suggesting that no increase in hydrogen crossover occurred. On the other hand, a combination of high temperature and reduced humidity promotes the degradation rate [72]. Studies of membrane stability at even more elevated temperatures (e.g., 120 °C) are often carried out at reduced humidity (<50%). It is expected that chemical degradation will be faster under these conditions than under ideal conditions. Hence, Asahi Glass has reported operation of a new membrane for 400 h without membrane failure or even significant fluoride release [73].

Desulfonation is generally studied by means of thermogravimetric analysis (TGA), differential thermal analysis (DTA), Fourier transform infrared spectroscopy (FTIR), and TGA-mass spectrometry (MS). In Nafion®-based composite, the decomposition behavior is attributed to the loss of sulfonic acid groups present in the unmodified Nafion® membrane [74]. The primary mechanism of degradation of these membranes is the degradation of the polymeric backbone; a secondary mechanism is the degradation of the pendant groups or inorganic compounds inside the membranes, which occurs at higher temperatures than primary degradation. Modification of polyaromatic membranes with acidic oxides results in an increase in membrane thermal stability at elevated temperatures. In efforts to improve membrane performance for high-temperature fuel cell applications, various polymers have been synthesized and tested for their proton conductivity, mechanical stability, electrode–membrane interface, and connectivity. These efforts, aimed at the commercialization of such membranes and the reduction of the cost of using PEM at elevated temperatures, seem to continue with insightful vision [3]. The future design concept of high-temperature PEMFCs will open new promising avenues for further research and development.

## 2.2 *Electrode and Catalyst*

In PEMFCs, as in the case of other low- or intermediate-temperature fuel cells such as the phosphoric acid fuel cell (PAFC) and the alkaline fuel cell (AFC), Pt and Pt alloys are the best electrocatalysts discovered to date for both hydrogen oxidation and oxygen reduction. In the types of fuel cells mentioned, the overpotential for the former reaction is considerably lower than that for the latter reaction. For example, in a PEMFC operating at a current density of 1 A/cm$^2$, the overpotential at the hydrogen electrode is about 20 mV while the overpotential at the oxygen electrode is about 400 mV. About one-half of the overpotential at the oxygen electrode is due to its loss at open circuit. The departure of the potential of the PEMFC from the reversible value is due to the extremely low exchange current density for oxygen reduction (about $10^{-9}$ A/cm$^2$) on smooth platinum electrodes. Due to this very low exchange current density value, competing anodic reactions are responsible for setting up a mixed potential of about 1.0 V for the oxygen electrode at open circuit. Oxygen reduction is considerably more complex than hydrogen oxidation due to (i) the strong O–O bond and the formation of highly stable Pt–O or Pt–OH species, (ii) the fact that it is a four-electron transfer reaction, and (iii) the possible formation of a partially oxidized species [43].

One of the major problems encountered with Pt electrocatalysis for hydrogen electrodes is its low tolerance to CO in $H_2$ from reformed fuels. Furthermore, according to the US Department of Energy, an increase in the cell potential to approximately 0.75–0.8 V is necessary for PEMFCs to compete with compression-injection direct ignition engines in order to meet the goal of 45% efficiency in fuel consumption. The improvement can only be achieved by

reduction of the oxygen overpotential by 50–100 mV. Recent studies have demonstrated that such an improvement is possible by using intermetallic electrocatalysts of platinum with a transition metal [75, 76], as used in state-of-the-art PAFCs.

The issue of carbon corrosion seems to be of even greater concern. Graphitic carbon is more stable than the conventionally used carbon black but has a lower surface area. This limits the minimum metal particle size, which in turn reduces the activity. In combination with the requirement for further reduction of the Pt loading, this is not a promising situation. Carbon corrosion may also be mitigated by promoting competing reactions. Development of catalysts for oxygen evolution has been suggested, but this concept is still unproven and may introduce new durability issues. The same holds for alternative supports. The electrode concept is based upon nonconductive organic whiskers coated by Pt [9]. In this concept, the support is not exposed to the electrolyte and Pt forms a continuous structure that is much less susceptible to dissolution and shows a high specific activity toward the oxygen reduction reaction (ORR). In spite of the low active surface area that is obtained and anticipated mass transport problems [77], may be a superior concept from durability point of view. Thus, in spite of recent research that has led to many new insights, testing protocols and characterization methods, improvement of fuel cell electrodes to meet existing durability targets still appears to be a formidable task.

## *2.3 Gas Diffusion Layer*

The gas diffusion layer (GDL) is responsible for the transportation of heat and gaseous phase, electronic contact, and water removal in a fuel cell. GDL consisting of carbon fibers, is a macroporous layer which has to some extent made hydrophobic by a Teflon coating. The microporous gas diffusion layer (MPL), which is positioned between the GDL and the catalyst layer, consists of carbon black particles and Teflon as a binder. Unlike the carbon black in the catalyst layer, the carbon black in the MPL is not susceptible to electrochemical corrosion and does not contain Pt to catalyze oxidation reactions but its chemical surface oxidation by water or even loss of carbon due to oxidation to CO or $CO_2$ cannot be excluded [78, 79]. These processes are responsible to increase hydrophilicity of the MPL. The carbon fibers of the GDL may be more stable but are otherwise susceptible to the same reactions. Decomposition of polytetrafluoroethylene (PTFE) used as a binder or hydrophobic coating has also been suggested. This idea was set forth on the basis of XPS data, but a mechanism has not been proposed [80].

As a result of chemical surface oxidation degradation, both the GDL and the MPL lose their hydrophobic character [80, 81] and the pore structure of the materials also changes. Both these phenomena have substantial effect on the water content of the GDL and MPL and therefore on their mass transport properties. Increased liquid water content of the GDL and MPL will impede gas phase mass transport because pores initially used for gas phase mass transfer will be

increasingly blocked by water. The relation between microstructure and surface properties on the one hand and mass transport properties on the other has been the subject of several recent experimental [13, 82] and modeling [83–86] studies. The results of these studies indicate that mass transport can indeed be seriously affected by the hydrophobicity of the GDL and MPL as well as by the pore size.

The properties of the GDL can also be changed by mechanical degradation arising from the compression forces in a fuel cell. From ex situ tests in which the material was aged under a compression force, it was concluded that compressive strain increased with applied pressure but even more strongly with temperature [87]. From this, it was concluded that GDL strain was influenced by PTFE stability. Properties such as in-plane electrical resistivity, surface contact angle, bending stiffness, and porosity were not affected. However, it was found that convective air flow through the GDL can lead to loss of material [58].

## *2.4 Membrane Electrode Assembly*

The membrane electrode assembly (MEA) is the 'heart' of the PEMFC and thus its structure and composition are of vital importance for the following reasons: (i) minimizing all forms of overpotential and maximizing the power density, (ii) minimizing the noble metal loading in the gas diffusion electrodes by high utilization of the surface areas of nanosized particles of the electrocatalyst (iii) for effective thermal and water management, and (iv) attaining the lifetimes of PEMFCs necessary for power generation, transportation, and portable power applications. Major progress in the designing of the MEA was made in the late 1980s and the early 1990s.

A breakthrough in achieving a tenfold reduction in platinum loading (from about 4 mg/cm$^2$ as used in the Gemini space flights to 0.4 mg/cm$^2$ or less in the PEMFC) in the 1980s and 1990s arose out of an invention [88] by workers at Los Alamos National Laboratory (LANL). The breakthrough was made possible by using platinum supported on high-surface-area carbon (e.g., Vulcan XC72R) as electrocatalyst rather than pure Pt black crystallites as in the Gemini fuel cells and by impregnation of a proton conductor (e.g., Nafion®) into the active layer of the porous gas diffusion electrode. The main factors that make it possible to reduce the platinum loading from more than 4 to 0.4 mg/cm$^2$ include (i) the considerably higher BET surface area of the carbon-supported electrocatalyst (particle size about 30 Å) than that of the unsupported previously developed PEMFC electrocatalyst (particle size about 100–200 Å) and (ii) extension of the three-dimensional zone in the electrode by impregnation of the proton conductor so that the utilization of the electrocatalyst might be similar to that in a fuel cell with a liquid electrolyte (e.g., phosphoric acid or potassium hydroxide).

In the late 1990s, significant increase in power densities with even further reduction in platinum loading to a level of about 0.05 mg/cm$^2$ for the hydrogen electrode and 0.1 mg/cm$^2$ for the oxygen electrode were achieved by deposition of

thin active layers of the supported electrocatalyst and proton conductor on an uncatalyzed electrode [89] or on the proton-conducting membrane [90]. These active layers are only about 10–20 μm in thickness and, unlike conventional electrodes, contain no Teflon. Because the active layers are considerably thinner than those of conventional electrodes (10 vs. 50 μm), the ohmic and mass transport overpotentials of the electrodes, which are generally predominant at intermediate and high current densities, are greatly minimized. An equally important advantage of such types of electrodes is the increase in platinum utilization from about 20–25% to 50–60%. The high utilization of platinum is essential from the point of view of reducing the platinum loading and hence the cost of the platinum in the electrode.

## 2.5 *Bipolar Plate*

Bipolar plates constitute the backbone of a fuel cell power stack, conduct current between cells, facilitate water and thermal management through the cell, and provide conduits for reactant gases, namely hydrogen and oxygen. In a PEMFC stack, the bipolar plates are key elements because they account for large fractions of the total weight, volume, and cost of the stack. Bipolar plates may represent up to 80% of the total weight and 45% of the total cost of a PEMFC stack [91]. Furthermore, these components perform vital functions in the stack such as carrying electric current away from each cell, distributing fuel and oxidant homogeneously within individual cells, separating individual cells and facilitating water management within the cell [92]. Because the plates perform such a number of functions, a variety of materials have been proposed for use in the manufacture of bipolar plates.

The gold-coated titanium and niobium used by General Electric for manufacturing bipolar plates in the 1960s, were substituted by graphite in the early 1970s because of its high corrosion resistance and low cost [44]. Graphite bipolar plates were manufactured starting from high-surface-area graphitic carbon powder mixed with ligand resins; after molding at high temperature and pressure, the gas distribution channels were introduced into the graphite blocks. However, due to the lack of graphite durability under mechanical shocks and vibration combined with cost effectiveness concerns regarding its high volume manufacturability, considerable research work is currently underway to develop metallic bipolar plates with high corrosion resistance, low surface contact resistance, and inexpensive mass production. Alternatives to pure graphite plates are composite bipolar plates based on the mixture of polymers and graphite particles. This class of materials allows mass production at a reasonable cost using manufacturing processes such as injection molding for thermoplastics [93]. There are several examples of graphite-based composite bipolar plates that use polypropylene (PP), polyphenylene sulfide (PPS), phenolic, or vinyl ester resins as matrices [94]. The polymer matrix gives flexibility to the bipolar plate, thus improving its mechanical strength. The chemical stability

is also not seriously affected by the incorporation of polymer in graphite. On the other hand, electrical conductivity is proportionally diminished because polymers are insulating materials. Thus, it is mandatory to formulate a composite bipolar plate with care so as to attain mechanical performance without sacrificing electrical conductivity.

In spite of the advantages of graphite-based composite bipolar plates associated with their low weight, high production, and chemical stability, comparison of the overall performance of graphite-based plates with that of metal bipolar plates reveals two major drawbacks, lower mechanical resistance and lower electrical conductivity. However, a handicap that may significantly decrease the performance of metal bipolar plates is their susceptibility to corrosion in the acidic and humid environment of PEM fuel cells. Metals operating in a fuel cell within a pH range of 2–4 and temperatures around 80 °C may suffer dissolution. The ions leached may poison the MEA, decreasing the power output of the fuel cell [95]. Furthermore, passive layers formed during operation increase the electrical resistivity of metal bipolar plates. Consequently, the fuel cell efficiency is negatively affected due to increasing interfacial contact resistance as the oxide layer grows. These effects offset the advantage of high electrical conductivity [96]. The problems outlined above may be minimized by protecting metal bipolar plates from corrosive fuel cell operating conditions with coatings [61]. A wide variety of alternatives have been proposed in research toward this objective.

## *2.6 Single Cell and Stack*

The wide range in power output of fuel cells implies significant variation in fuel cell operating conditions, active area, gas diffusion media, bipolar plate, and MEA properties. The performance of a PEMFC stack varies significantly with respect to the number of cells, operating conditions, material properties, and flow-field characteristics. Understanding how the PEMFC stack performs, including the transport behavior of each particular design with respect to overall performance analysis and the local examination of electrochemical variables, temperature and water distribution, will lead developers toward improved designs and enhanced durability. This understanding requires both experimental study and numerical analysis [97]. The 55-partner-strong FCTESTNET thematic network was established to define harmonized test procedures applicable to the component level (single cells, multi-cell stacks, Balance of Plant or BoP), subsystems, and entire fuel cell systems. The purpose of this test module was to characterize the performance of a PEMFC stack under constant current conditions. The module is used for measuring the voltage and power of a stack as a function of drawn current. If properly instrumented, cell voltages, different temperatures, reactant flows, relative humidity, stack fluid pressures, and pressure drops can be measured. These modules are accessible at the FCTES$^{QA}$ website [98].

### 2.6.1 Water and Heat Management

Water plays an important role in fuel cells. Its functions in fuel cells include as a reactant at the anode in the creation of protons, hydrating the PEM membrane to promote proton transport toward the cathode, and representing a product of the consumption of those protons at the cathode. The flux of water toward the anode under fuel operating conditions can lead to so-called 'water flooding,' requiring a balance between membrane hydration and flooding avoidance [99]. The maximum degree of hydration of the membrane electrolyte is vital for the PEMFC to attain its highest performance. If sufficient hydration is not achieved, the ohmic overpotential in the membrane could be a major source of loss of efficiency in the PEMFC. The flux of water is measured by the electro-osmotic coefficient, which equals the ratio of the number of transported water molecules to transported protons. With improvements due to the invention of Nafion®, the electro-osmotic drag coefficient of water in a fuel cell is about 2.5. Thus, because the oxidation of 1 mol of methanol in the presence of water at the anode generates 6 protons, 2.5 × 6 mol of water will be dragged through a Nafion® 117 membrane toward the cathode. This value will be higher if the membrane is equilibrated in a water-methanol mixture [100], in which the loss of 16 water molecules from the anode occurs for every mole of methanol oxidized.

The potential applications of PEMFCs in electric vehicles have stimulated the development of internal hydration techniques. In these techniques, the water produced by the electrochemical reaction is used for the hydration of the membrane, allowing the elimination of an external humidification subsystem. This method can also reduce the volume and weight, and thus the size, of the overall system. Several methods have been proposed which include (i) the use of porous carbon blocks for the bipolar plates (due to capillary condensation, such plates are able to retain the water produced by the electrochemical reaction and also assist water transport from the cathodic to the anodic side of the fuel cell) in this type of cell stack, the carbon blocks are not channeled, and the gases are humidified by forcing them to flow through the wet porosities [101]; (ii) impregnation of the membrane solution into the electrode, forming a thin recast film on the surface, followed by hot-pressing of two impregnated electrodes onto each other; with this procedure, very thin electrolyte films that show very small ohmic resistance and thus allow operation even under unfavorable conditions, such as low pressure and temperature and without external humidification, can be prepared; and (iii) impregnation of thin Nafion® recast membranes with a small amount (approximately 5–6 wt%) of nanosized Pt particles. In this case, Pt catalyzes the production of water from the crossover flux of $H_2$ and $O_2$ across the membrane, thereby ensuring a satisfactory hydration level [102].

Proper thermal management is also recognized as a critical issue in the commercialization of PEMFCs. The ambient temperature directly affects the heat exchanger fan power consumption and the maximum power, with a statistically significant effect on net efficiency [103]. PEMFCs are operated at temperatures in the range of 70–80 °C to prevent dehydration of the PEMs. A cell temperature below 60 °C leads to water condensation and flooding at the electrodes,

accompanied by voltage loss. These stringent thermal requirements present significant heat transport problems. Heat generation in PEMFC arises from the entropic heat of reactions and the irreversibility of the electrochemical reactions and ohmic resistances, as well as from water condensation [104]. Thermal management in a DMFC is intimately tied to the water and methanol-transport processes. The heat generation in DMFCs is comparatively higher than in PEMFCs due to lower energy efficiency (20–25% at 0.3 and 0.4 V). High-cell temperatures promote methanol oxidation and increase the methanol crossover rate, which reduces fuel cell efficiency and energy density.

### 2.6.2 Fuel Crossover, Oxidation, and CO Poisoning

There are two technical challenges for PEMFC technologies: (i) high methanol crossover ($10^{-6}$ mol/cm$^2$ s) and its further reaction with the Pt catalyst sites on the cathode, which reduces the fuel cell efficiency (50–100 mA/cm$^2$) [105]; (ii) insufficient activity of the anode catalyst, which results in high overpotential loss (about 350 mV) for DMFC compared with that for PEMFC (60 mV) [106]. Slow anode kinetics due to methanol crossover reduces the power density of DMFC approximately 3–4-fold in comparison with a hydrogen fuel cell [104]. Pt–Ru and several other anode catalysts have been developed [107, 108], and their effects on electrochemical anode reaction and cell performance have been experimentally studied [109].

The presence of CO in the fuel gas (sometimes termed CO poisoning) degrades PEMFC performance by its preferential adsorption on the platinum surface, resulting in blockage of active sites. The following three methods were reported to mitigate CO poisoning effects: (i) the use of a platinum alloy catalyst; (ii) higher fuel cell operating temperature; and (iii) introduction of oxygen in the fuel gas [110]. The poisoning effect is temperature dependent, being less pronounced at high temperature [111]. To avoid CO poisoning, PEMFCs require operation in pure hydrogen and DMFCs must be operated at high temperature with an efficient electrocatalyst.

In addition to the problems discussed above, various other factors also affect fuel cell performance; these include membrane dehydration, reduction in membrane conductivity, and mechanical stability [112]. Also, under oxidizing conditions, free radicals (oxygen, hydroxide, and peroxide) attack the alkyl chains of the membrane, resulting in loss of functionality and reduced overall membrane performance. Thus, for successful fuel cell operation, membranes that are highly thermally, mechanically, and oxidatively stable over a wide pH range are urgently required.

### 2.6.3 Scale-up and Long-Term Experiments

Unlike other types of fuel cells, PEMFCs show some loss of efficiency and power density with scale-up in the area of the electrodes and the increase in number of

cells in a stack. The main reason for this is that removal of the product (i.e., liquid water) becomes more difficult in larger systems. Furthermore, a high water vapor pressure in the reactant flows causes an increase in overpotential, especially at the cathode [113]. An issue strongly related to water management is that of thermal management in stacks. On one hand, temperatures that are too low cause water condensation problems, as discussed above. On the other hand, an even more important factor is that high-cell temperature, even in confined areas, leads to membrane dehydration and consequent loss of performance. Although a PEMFC is a very efficient system, 40–50% of the energy produced is still dissipated as heat. This loss of electrochemical performance is due to the irreversibility of the cathodic reaction, to ohmic resistance and mass transport overpotentials. To prevent drying out of the membrane and the rise in the cell temperature, the generated heat must be removed from the cell. Because the temperature difference between the cell and the surroundings being approximately about 50 °C, it is impossible to rely on natural convection and air cooling for efficient heat removal [114].

Fuel cell and stack design engineering aimed to improve the performance of devices in terms of power density and specific power. Single cell design is realized on the basis of experimental purposes. In addition, fuel cell stacks are often designed for worldwide applications in order to reach enough power. However, stack design is more complicated because power and overall voltage target must be taken into account and MEA loss of performance must be minimized. Moreover, the stack final application, specific geometrical requests and the cooling system must also be considered [115]. Consequently, innovative PEMFC stack research involves all the components of the stack from the membrane to stack auxiliaries, with special attention to materials, hardware design (channels geometry, manifold, sealing, and the like) and fuel cell component coupling.

The polarization curves of an $H_2/O_2$ single cell with a composite membrane are shown in Fig. 4. It is obvious that the performance of the single cell reached its maximum at 60 h and then degraded significantly during subsequent testing.

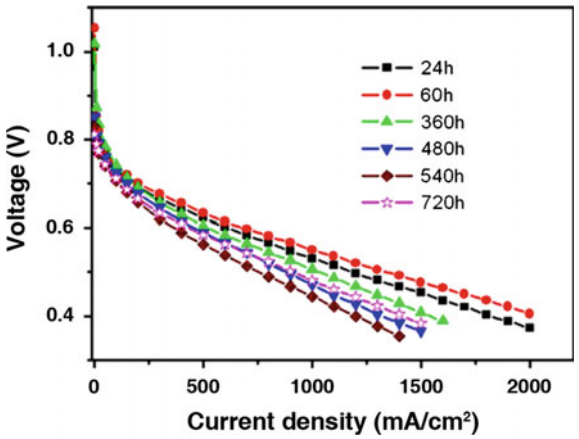


**Fig. 4** Polarization curves of the $H_3PO_4$/Nafion®-PBI composite membrane single cell at different test times. *Source* Ref. [60]

For example, the single cell voltage at 1000 mA/cm$^2$ fell from 0.55 V at 60 h to 0.45 V at 540 h, although it increased slightly at 720 h. The degradation in the performance of the single cell during the test resulted from degradation of the electrocatalyst and the membrane [116]. The small increase at 720 h appears due to an increase in the membrane proton conductivity resulting from the increased permeability of the membrane [117]. The long-term stability of membranes under different operating conditions can also be examined. In short, MEA testing will be of great advantage in fine-tuning the properties of hybrid membranes to establish their commercial viability. However, a major technical challenge is the scaling up single cell performance to stacks [65].

Long-term experiments can be indicator of the severity of degradation of membranes and relative contribution to performance loss under various conditions. The compilations of PEMFC experiments longer than 1000 h are meant to give a qualitative understanding of the possible relationship between operating conditions and voltage decay rates; such tests are difficult to compare quantitatively because of differences in materials, flow-fields, start-up procedures, and other parameters. Note that the voltage decay rates comprise irreversible as well as reversible losses. In durability studies, it must always be remembered that part of the decay may be reversible. This is particularly true in the case of under- or over-saturation of the gases. Both drying out and flooding can have a detrimental effect. During a 26,000 h test conducted by Gore [118], a voltage loss of 110 mV was observed at a current density of 800 mA/cm$^2$. The sensitivity of a fuel cell system to dual-stack parallel and series array operation has been evaluated experimentally. The system net efficiency was lower for the parallel arrangement than that of the series arrangement because connecting the stacks in parallel equalized the stack voltages. The weaker stack depresses the polarization curve of the stronger stack, while the stronger stack boosts the polarization curve of the weaker stack [119].

## 3 Structured Techniques for Flow-Field Optimization

The performance of a PEMFC is primarily determined by the intrinsic electrochemical efficiency of the MEA. Nevertheless, other factors such as flow-field design, thermal and water management, and operational control are also important [51]. The flow plate is one of the key components of a PEMFC and serves as both the current collector and the reactant distributor. The reactants, as well as the products, are transported to and from the cell through the flow channels. The essential requirements for the flow-field are uniform distribution of reactants over the entire electrode surface and effective removal of products from the cell, to minimize the concentration polarization. Flow plates contain either a few very long channels or a large number of channels. These channels make up the flow-field through which the reactants are distributed to the entire surface of the MEA. An optimal flow-field design is critical for obtaining high power density in a fuel cell and thus is extremely important. Since the early development of PEMFCs,

variety of flow-field designs has been introduced. Generally three major types of flow-fields are in use: parallel, serpentine, and interdigitated. The serpentine flow-field is the most commonly used [2].

Much efforts have been put forth to design an optimum flow-field for PEMFCs that can both efficiently distribute reactants to the reaction sites and remove products through the outlet. The presence of water in the products has been one of the main concerns. To operate a PEMFC within a narrow band of water content is a challenging task considering the vast range of power demand and environmental conditions that pertain to vehicular applications. This makes the design of the gas channels a very critical factor. Under different flow rates, relative humidities of air intake and different current demands, complex two-phase flow regimes have been observed in the gas channels. Therefore, it is essential to design blockage-resistant gas channels with an acceptably small power loss to pump fuel and oxidant.

Data from a set of investigations on flow-field optimization that include both experimental [39, 63, 98, 120–137] and modeling approaches [59, 68, 138–157] to achieving uniform distribution of reactants were analyzed with the validation of experimental and numerical results [97, 158–161]. The subject of these investigations ranged from single cells to stacks in PEMFCs. These studies, which are schematically shown in Fig. 5, are being described in this section in order to provide guidance to the optimization of flow-field design for efficient operational control in PEMFCs.

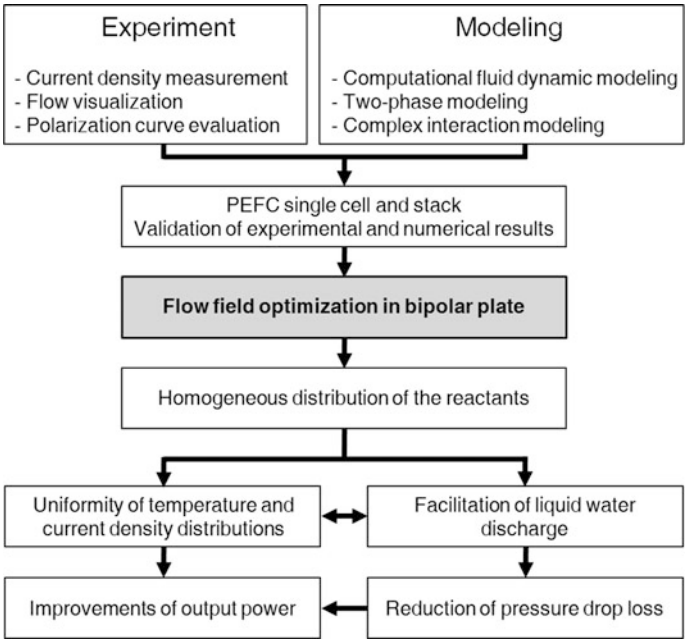


**Fig. 5** Flow diagrams for the optimization of flow-field in PEMFCs

## 3.1 Experimental Approaches to Flow-Field Optimization

### 3.1.1 Current Density Measurement

It is desirable to operate a PEMFC at uniform current density over the MEA because nonuniform current distribution in a PEMFC could result in poor reactant and catalyst utilization, low energy efficiency, and possible corrosion inside the fuel cell. Local current distribution in a fuel cell can be strongly affected by the operating conditions as well as by the organization of the reactant flow arrangement between the anode and cathode streams, especially in practical PEMFCs of large cell size [120]. For instance, reactant depletion along the flow channel leads to current variation from the channel inlet to the exit and degrades the cell performance and flow arrangements between the anode and cathode streams, such as co-, counter-, and cross-flow, can exacerbate this effect considerably, resulting in complex current distribution patterns over MEA surfaces. During normal PEMFC operation, nonuniform current distribution cannot be measured directly because only integral values such as cell voltage, current density, and impedance can be measured. Therefore, considerable effort has been made to measure and understand the current density distribution in PEMFCs using a variety of approaches.

The segmenting flow-field is one of the most popular techniques for measuring the current distribution in PEMFCs. This technique measures the current distribution in a PEMFC using a segmented bipolar plate and printed circuit board. The anode GDL and catalyst layers were also segmented. Three other segmentation methods were also proposed; these included a partial MEA approach, current mapping, and the use of sub-cells to measure the current distribution [121]. Using the same principles, the current distribution was measured along the length of a single flow channel in a PEMFC with higher resolution of spatial and time. The time delay of local currents was observed after inlet reactant gas changes due to the mass transport of gas through GDL. Simultaneous measurements were made for species concentration and current distribution. Furthermore, a PEMFC permitting simultaneous evaluation of current, temperature, and water distribution in the cell under various operating conditions was designed [122, 124]. Consequently, the experimental setup allowed to perform a simultaneous evaluation of current, temperature, and water distribution in a polymer electrolyte fuel cell under operation. The test fuel cell has a segmented anode flow-field for current distribution measurement. The cathode end plate was made of an optical window, which was transparent for infrared as well as for visible wavelengths. This allowed infrared thermography and optical surveillance of water droplets and flow-field flooding.

The uniformity of current density distribution was evaluated experimentally using third single cells and the PEMFC test station developed and installed at Power System and Sustainable Energy Laboratory of INJE University, as shown in Fig. 6 for quantitative analysis in performance test of PEMFC. As shown in Fig. 6, reaction gases such as hydrogen and oxygen must be carefully moved from the container to the entrance of fuel cell without any changes of temperature, pressure,

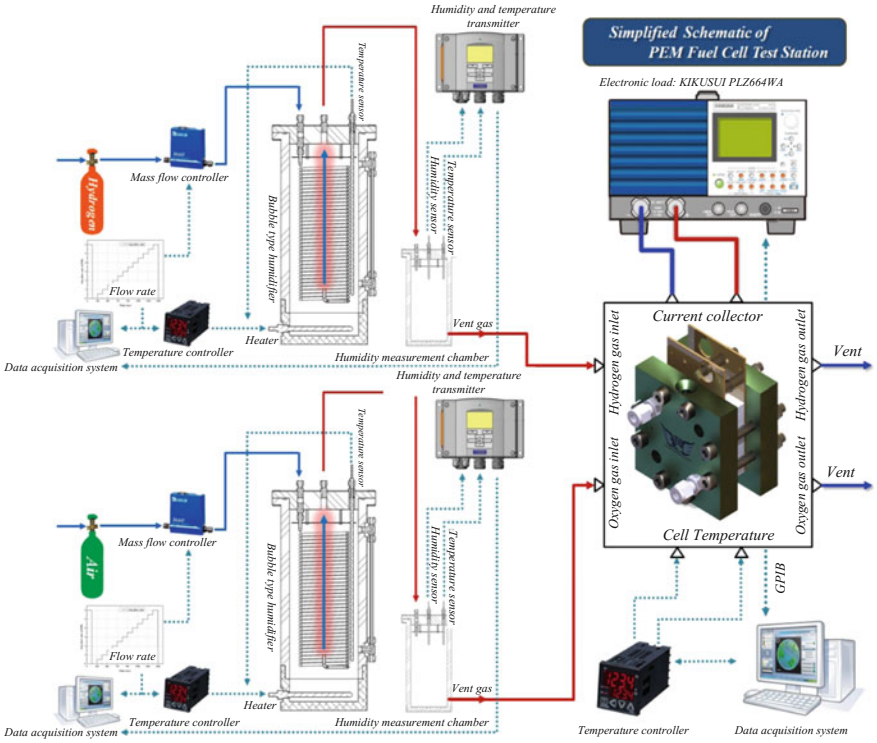


**Fig. 6** Schematic diagram of the main experimental modules installed at Power System and Sustainable Energy Laboratory of INJE University

and flow rate. The performance of PEMFC is greatly affected by temperature, pressure, flow rate, and humidity. The segmented current collector was inserted between the back side of the anode flow-field plate and the current collector, as shown in Fig. 7. The graphite block is filled with an electrically insulating epoxy between the anode bipolar plate, the sensor plate, and the current collector to minimize electrical contact resistances [123].

Other techniques for measuring local current distribution in PEMFCs have been reported in the literature. The potential distribution at the interface between the GDL and the catalyst layer (CL) was measured to obtain sub-millimeter resolution of the current distribution measurement [125]. This research provided useful insight into mass transport issues in land and channel areas of the flow-field plate. A novel approach was developed to measure current densities under the channel as well as under the land separately in PEMFCs with a parallel flow-field. The cathode catalyst layer was designed to have either the area under the land or the area under the channel loaded with catalyst. This design yielded separate measurements of current densities under the land and the channel. An optimization study of current density

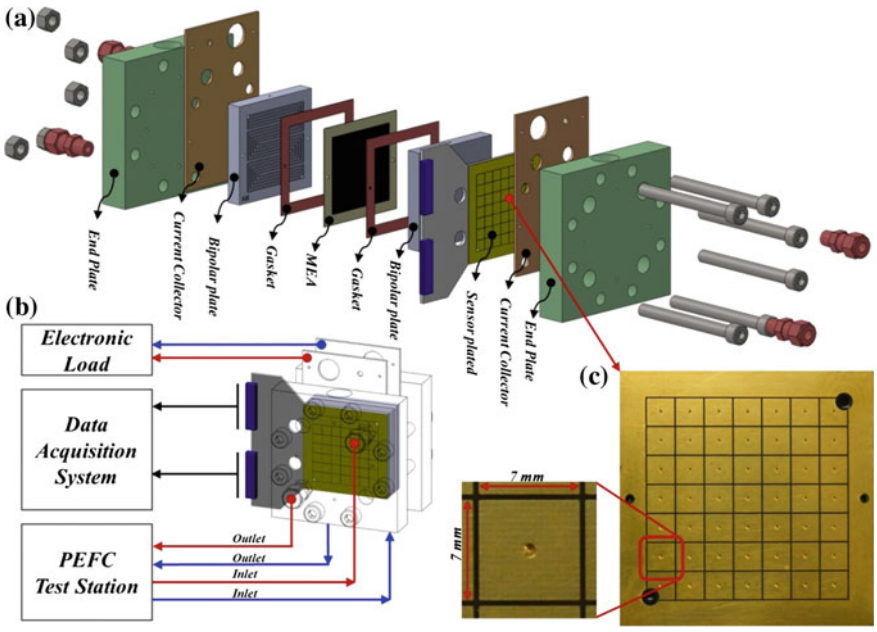


**Fig. 7** Schematic of the experimental setup with the segmented Bipolar Plate installed at Power System and Sustainable Energy Laboratory of INJE University

distribution under the land and channel areas was conducted for a variety of serpentine flow-field geometries and operating conditions [126].

It is clear that considerable effort has been devoted to developing methods for current distribution measurements in PEMFCs for various reactant flow arrangements and under different operating conditions such as varying stoichiometry ratio, reactant pressure, cell temperature, and relative humidity. Currently, the local current distribution in a PEMFC with different flow arrangements and operating conditions is most often measured using the segmented bipolar plate or printed circuit board technique [127]. The design of the flow-field greatly affects the flow distribution and the final performance of the PEMFC system. An optimization model that takes the effect of the GDL deformation into consideration was proposed to obtain more uniform flow distribution for the flow-field configuration design [128]. It was found that the GDL deformation must be taken into consideration in the optimization of the flow-field due to its great influence on the flow distribution. In addition, both the uniformity of the flow-field and its sensitivity to the GDL intrusion should be considered in order to obtain a robust design. From the optimization results, it can be seen that in order to achieve more uniform flow distribution and high performance, the slots in the central channels should be shallower and wider than those in the side channels.

### 3.1.2 Flow Visualization

In PEMFCs, insufficiencies in the proton network and membrane degradation can occur as a result of drying of the membrane. Excess water, on the other hand, blocks gas flow channels and hinders gas access to active catalyst areas, resulting in significant drops in performance. Water management is, therefore, one of the most important issues in the design of PEMFCs. Oxygen partial pressures and water blockages were visualized simultaneously in a triple serpentine PEMFC, and the relationship between the two was investigated [129]. Air can be supplied from the other channels through the GDL, and power generation continues at the catalyst layer, even under the blocked channel. Thus, water continues to be produced at the catalytic layer under the channel blocked by water. The water layer produced at the catalytic layer under the blocked channel might not be easily removed because of the limitation of gas flow due to the blockage. In this situation, even though the water droplet in the channel is ejected from the cell, the catalyst layer is still wet; thus, the oxygen consumption is low in the channel and thus the oxygen partial pressure remains high. Such a flooded area may expand with operation time, causing significant performance and efficiency losses in the fuel cell, as shown in Fig. 8.

Novel diagnostic techniques designed especially for the visualization of water have been intensively applied to PEMFCs to elucidate the nature of water transport inside the cell. There has been a rapid and continual growth in the number of publications on in situ and ex situ visualization techniques in PEMFCs. These publications cover topics such as magnetic resonance imaging, neutron radiography, X-ray imaging, fluorescence microscopy, infrared visualization, and direct optical visualization. These techniques play complementary roles in achieving an understanding of water transport in PEMFCs because each technique has an individual capability of detecting the presence of water in different materials at different spatial and temporal resolutions. The state of the art in relation to in situ

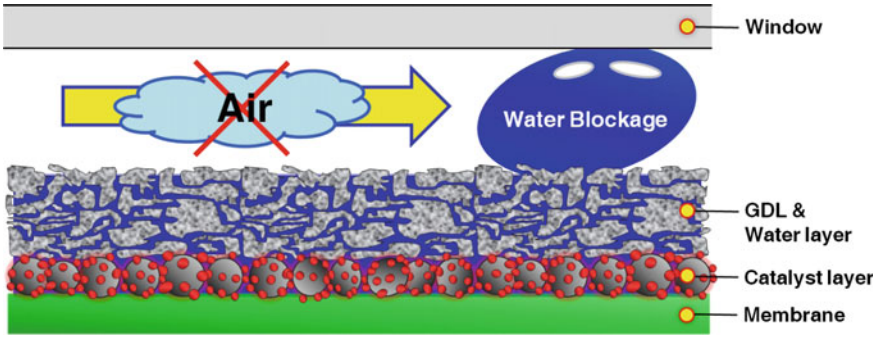


**Fig. 8** Schematic drawing of the channel, gas diffusion layer, and catalyst layer with water blockage. *Source* Ref. [128]

visualization techniques for use as diagnostic tools in studies on water transport in PEMFCs has been comprehensively reviewed [63].

Because of the importance of water transport to the functioning and efficiency of fuel cells, many researchers focus on water transport mechanism and water equilibrium technique in PEMFCs. For liquid water transport in gas channels of PEMFCs, direct observation of transparent method has been conducted by many researchers. The influence of operating conditions on liquid water formation and the fuel cell performance is one point that is often emphasized. During the start-up and shut-down processes of a PEMFC, platinum particles are lost from the catalyst layer at the cathode due to corrosion of the carbon supports. During gas exchange, the distribution of oxygen partial pressures at the anode was visualized using our real-time/space visualization system, which clearly showed the location of $H_2$- and $O_2$-rich areas along the gas flow channel from the inlet to the outlet. The gas exchange rate was found to be much slower than that predicted from simple replacement. In addition, it was also related to the proton transfer derived from carbon corrosion of the cathode catalyst layer. From the visualization results, it was found that the shut-down process produces a more serious effect than the start-up process. The oxygen partial pressure at the cathode was visualized during cell operation after degradation. Because the MEA was degraded mainly near the inlet and outlet of the reactant gases in the cell, oxygen was consumed primarily in the middle of the MEA [130]. Transparent acrylic materials were used to make various fuel cell models for the experiments. The parameters considered in the experiments were the rate of water injection into the models, the velocity and temperature of the humidified gas in the cathode channels, the type of flow-field, and the temperature. It was found that the parallel and interdigitated flow channels were easily flooded under certain conditions. Fuel cells with two different types of flow channels and two different electrode sizes were made, and their performances were compared with some of the flooding results obtained from the transparent physical models [131].

The effects of four operating parameters, namely air stoichiometry, hydrogen stoichiometry, cell temperature, and electric load, on the formation and extraction of water from flow channels were investigated [132]. These results showed that hydrogen and air stoichiometry contributed almost equally to the process of water formation of water in the cathode channels. However, contrary to hydrogen, changing the air stoichiometry proved capable of extracting all the water from the cathode channels without dehydrating the membrane. Increasing the operating temperature of the cell was found to be very effective in the water extraction process; no water was present in the anode flow channels under any of the examined operating conditions. The liquid water flow patterns in the fuel cell gas channels and GDLs were also addressed by the researchers. Visualization of the two-phase flow occurring at the anode side was carried out using fluorescence microscopy. In correlating the observed flow patterns with the corresponding current density of the polarization curve, a strong influence of the two-phase flow on the performance of a fuel cell at high current densities became apparent. The functionality of a flexible direct methanol micro-fuel cell was also investigated under different bent conditions. The tests showed an insignificant drop in electrical

performance under bending due to an inhomogeneous contact resistance. Characteristics of liquid water removal from GDL were investigated experimentally by measuring the nonsteady pressure drop in a cell in which the GDL was initially wet with liquid water [133]. The thickness of the GDL was carefully controlled by inserting metal shims of various thicknesses between the plates. It was found that severe compression of the GDL could result in an excessive pressure drop from channel inlet to channel outlet. Removing liquid water from GDLs with high compression levels and low inlet air flow rates by cross-flow is difficult. However, effective water removal can still be achieved at high GDL compression levels if the inlet air flow rate is high. Water removal characteristics due to the cross-flow through the GDL at different levels of compression were investigated for a transparent cell with a serpentine flow channel layout. Experimental measurements revealed that the total pressure drop from the channel inlet to the channel outlet is reduced substantially when compared with the case without the GDL [134]. These studies show that flow visualization under the land area confirms that the cross-flow has significant effects on water removal even at low air flow rates. Thus, the effects of cross-flow and the compression level of the GDL should be considered in the design and optimization of practical PEMFCs.

Visualization of liquid water transport has been conducted using transparent flow channels, and liquid water removal from GDL under the land was observed for all the tested inlet air flow rates, confirming that cross-flow is practically effective in removing the liquid water accumulated in GDL under the land area. To date, there have been few publications that focused on direct observation of liquid water flow state at the turns of gas channels of PEMFCs. In fact, literature concerning the relationship among the liquid water production rate, the fuel cell internal resistance and performance is hardly found. However, water transport in the channels of transparent PEMFCs has been studied under different operating conditions using a high-speed camera [135]. First, the spot distribution for liquid water droplet emergence in the channels of transparent PEMFCs with multi-straight channel flow-fields was observed and analyzed; second, the flow state of liquid water at the turns of a transparent PEMFC with serpentine channel flow-field was studied under different gas flow rates; finally, the water transport in a transparent PEMFC with a multi-straight channel flow-field was examined. The fuel cell performance and the internal resistance were measured under different operating conditions, the liquid water accumulated in the gas channels was simultaneously recorded and estimated, and the relationship among the fuel cell performance, the internal resistance and the liquid water mass accumulated in the channels was analyzed. This work led to some beneficial conclusions.

### 3.1.3 Polarization Curve Evaluation

The performance of a fuel cell is mainly characterized by its polarization curve (a plot of cell potential versus current density). In polarization curves, three different regions are observed that correspond to different phenomena (electrochemical

kinetics, ohmic resistance, and reactant mass transport) limiting the cell potential, which depends on the current density being drawn (Fig. 3). The test is used to determine the performance of a PEMFC stack and the stability of test input and output parameters as a function of test duration, current density, and stack power [98]. At minimum, stability criteria for the stack current, the stack temperature and pressure, and the stack voltage should be defined and stated in the test report. The stability check of the test outputs should follow the stability check of the test inputs. If all stability criteria are fulfilled, the verification may also be carried out offline during data post-processing.

The polarization curve test method was used to investigate a non-isothermal tapered flow channel installed with a baffle plate for enhancing cell performance in the cathodic side of a PEMFC. The effect of parameters including tapered ratio (0.25–1.0) and gap ratio (0.005–0.2) on cell performance were explored in detail [39]. The results indicate that the stronger composite effect of tapered flow channels and baffle blockage provides better convection heat transfer performance and higher fuel flow velocity and thus enhances cell performance. The effects of three different anode and cathode flow-field designs (single serpentine (SFF), multi-serpentine (MSFF), and an original mixed parallel and serpentine design (MFF)) on the performance of a DMFC was investigated experimentally. The studies were conducted on a DMFC with 25 $cm^2$ of active membrane area, working near ambient pressure and using two values of methanol concentration, fuel cell temperature, methanol, and air flow rate. With respect to the anode flow-field design, it was found that the use of MFF has a positive effect on cell voltage and power at the two values of methanol flow rate tested, at the lower value of fuel cell temperature and at the lower value of methanol concentration [136]. However, in case of the cathode flow-field design, MSFF leads to a better. For the higher value of methanol concentration tested, a very important condition for portable applications, the use of MSFF or MFF as anode flow-field design and MSFF or SFF as cathode flow-field design produces enhanced fuel cell performance. Most of the reported experiments were conducted close to room temperature, thus providing information and results that can be used for designing a portable DMFC to be used under less severe operating conditions.

AC impedance spectroscopy is helpful for measuring different fuel cell parameters and for understanding the limiting processes affecting overall fuel cell performance, as well as for cell state-of-health determination. Experimental performance results, including polarization curves and Electrochemical Impedance Spectroscopy (EIS) analysis of the fuel cell, were obtained for a 50-$cm^2$ PEMFC [137]. A cell with a serpentine flow-field was found to perform better than a cell with a parallel flow-field. In the former, the polarization curve was higher and the membrane and contact resistances were lower. Fuel cell operation with pure oxygen improved the performance parameters as well. The resistance of the oxygen reduction reaction at the cathode was found to be significantly lower when operating with pure oxygen. Reactant gases humidification also improved cell operation, resulting in higher polarization curves and membrane conductivities and preventing the MEA from drying out. A special tubular cathode has been prepared using graphite-doped

mesocarbon microbeads (MCMB/G), dip-coating the gas diffusion and catalyst layers with subsequently wrapping the sintering tube with the Nafion membrane. The sol-gel flux phase was prepared using sol-gel technology. The impedance of the specially shaped DMFC with a sol-gel flux phase was investigated and the effects of tube wall thickness, gas diffusion layer loading, working temperature, and sol viscosity on the cell polarization performance were examined [138]. The results showed that the impedance of the specially shaped cell was much higher than that of the traditional flat electrode; however, an obvious decrease in impedance was observed after activation. The cell performance improved with the decrease in sol viscosity and with the increase in working temperature.

## *3.2 Modeling Approaches to Flow Optimization*

### 3.2.1 Computational Fluid Dynamic Modeling

Because of the many difficulties involved in observing and measuring species movement and distribution inside a PEMFC, numerical modeling has become an indispensable research tool in the design and assessment of PEMFCs. The first application of computational fluid dynamic (CFD) methods to PEMFCs focused on a one-dimensional model that included several important principles related to the electrochemical reaction process that occurs in fuel cells [68]. Two-dimensional models that emphasize the effects of two-phase water and heat transport have also been developed by some researchers. Although two-dimensional models represent significant advances in fuel cell modeling, the transport processes that occur in a PEM fuel cell are intrinsically three dimensional. Therefore, it is not possible to accurately predict cell performance unless a realistic, three-dimensional description of the cell geometry is considered. Two-dimensional models are inadequate because they only consider areas where cell efficiency is the highest thus; these models strongly overestimate the limiting current unless heavy model tuning is performed. Obviously, this impedes their use as design tools. Recently, two-phase numerical models that incorporate the coupled effects of electrochemical reaction and mass transport in three-dimensional domains have been developed by many researchers [59]. These models are extremely complicated because they take into account the biphasic phenomenon which occurs at high current density (>1 A/cm$^2$) and offers a small effect on cell performance. This high current interval is characterized by power drop and is therefore less used in industrial applications.

Common flow-field patterns include serpentine, parallel, interdigitated, and straight patterns (see Fig. 9) as well as their combinations. A three-dimensional single-phase isothermal model was developed to describe the steady-state and transient response of four PEMFCs with different flow-field designs including serpentine, parallel, multi-parallel, and interdigitated types [139]. The modeling results showed that the transient responses of serpentine and parallel designs were faster but the performances were lower than those of the other two designs.

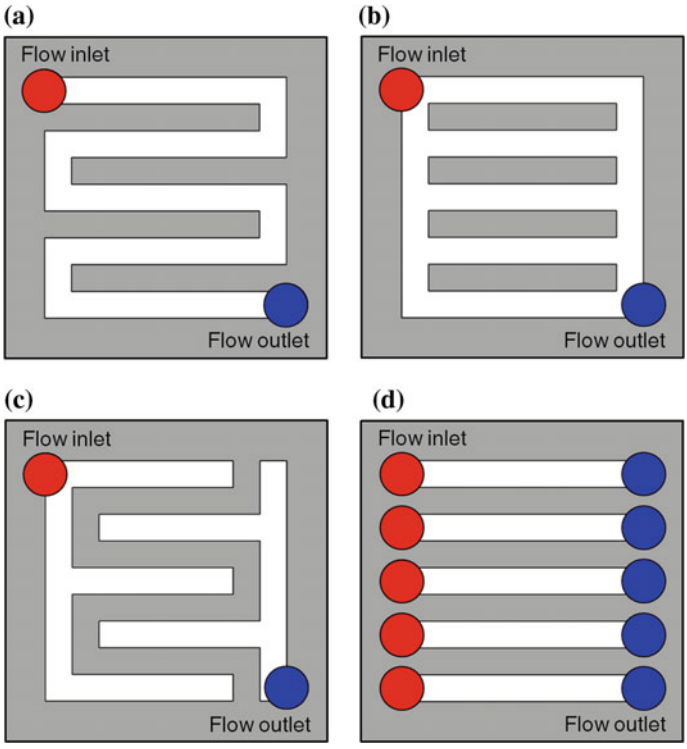


**Fig. 9** Major flow-field patterns of PEMFCs: **a** serpentine; **b** parallel; **c** interdigitated; **d** straight. *Source* Ref. [4]

However, this study did not consider water accumulation in the GDLs. Due to the heavy computational method employed; the model was not able to simulate PEMFCs with different anode and cathode flow-field designs. Lumped models that assume uniform reactions within the entire area of the fuel cell do not consider the spatial distribution of reactants. In practice, fuel cell performance and water distribution depend on flow-field design. Moreover, water generation and accumulation inside the fuel cells are distributed unevenly along the flow channels. A model that can describe the distributed properties of a single cell, especially that of a cell with a complex flow pattern, is needed. In order to solve this problem, a segmented model was developed to predict the distribution of liquid water accumulation, current density, membrane water content, and relative humidity in the flow channels [140]. In the segmented model, three single cells with different flow-field patterns are designed and fabricated. These three flow-field designs are simulated using the model, and the predicted results are validated by comparison with experimental data. The segmented model can be used to predict the effect of flow-field patterns on water and current distributions before the cells are machined. Under low-humidity working conditions, the current density of the first segment, which is near the inlet,

takes approximately 3.9% of the current load in traditional flow-field designs. The value can be improved to 4.7% by placing the cathode flow direction opposite to the anode. The counterflow design also results in a more uniform distribution of water content in the membrane; thus, the durability and efficiency of the fuel cell can be improved.

In a DMFC operated at ambient temperature, electrochemical reactions generate large amount of carbon dioxide at the anode side, while liquid water is produced at the cathode side. Studies using different flow-fields have compared the influence of the flow-field design on the performance of DMFCs. These studies concluded that flow-field patterns can significantly affect the distribution of gas flow and current density within a DMFC. The effect of anode flow-fields on the behavior of methanol and carbon dioxide in DMFCs has been extensively studied. DMFCs with single serpentine flow-fields (SSFF) showed better performance than those with parallel flow-fields (PFF). Besides the SSFF and the PFF, the grid flow-field (GFF) was introduced into DMFCs; the performance of DMFCs with different flow-fields, from best to worst, was SSFF > GFF > PFF [141]. Comparisons between SSFFs and PFFs in micro-DMFCs also show that DMFCs with SSFF have better performance than those with PFF. The behavior of micro-channels, which is different from that of conventional larger channels, was studied at the corresponding Reynolds number. Flow-fields with micro-channels need to be further investigated in micro-DMFCs [142]. Flow-fields and membrane electrolyte assembly (MEA) providing a 2.25-$cm^2$ active area were assembled in micro-DMFCs. These micro-DMFCs yielded maximum power densities ranging from 11 to 23 $mW/cm^2$ for methanol solution concentrations of 1, 2, 3, 4, and 5 M at a temperature of 20 ± 1 °C. The maximum power densities observed imply that under the ambient temperature and low flow rate of methanol solutions, the performance of micro-DMFCs with different flow-fields ranked as double-channel serpentine > single-channel serpentine > mixed multichannel serpentine with wide channels > mixed multichannel serpentine with narrow channels [143].

A complete three-dimensional simulation based on a single domain approach for species transport in PEMFC with straight flow channels was examined [144]. Numerical simulations show that water vapor is mainly concentrated in the gas diffusion layer under the current collecting land due to the deceleration created by collector contraction effects, but the water vapor is still far from the catalyst layer. This result draws more attention to the role played by the porous media of GDL, which prevents severe liquid flooding on the cathode side. Oxygen concentration in the reaction sites is significantly affected by an increase in pressure, which increases the power of fuel cells but also requires more auxiliary energy consumption, which must be reduced from the power of the cells' output. One of the critical issues in developing efficient PEMFCs is to achieve better water management within the MEA. Although electrochemical reactions are only feasible in moist environments, excessive liquid water blocks the passage of air into the active sites of the catalyst layer. Because explicit water front tracking is unnecessary with single domain formulations, fewer complexities exist in mathematical modeling as well as fewer difficulties in computations, especially for high-dimensional problems.

A new method of single domain formulation, termed the pseudo-phase-equilibrium approach, has been recently proposed [145]. The validity of the pseudo-phase-equilibrium approach was evaluated over an extensive polarization range under specified operating temperature, pressure, and inlet humidity conditions. The solutions obtained using the pseudo-phase-equilibrium approach and the exact phase-equilibrium equations were compared over a wide range of parameter values. In addition, the influences of important transport parameters such as water transport coefficient, gas diffuser porosity, and absolute liquid permeability have been evaluated.

The fundamental algorithms and methods described here have been used for decades, have proven to be very efficient, and are being used by many modeling groups along with user-defined coding. One cannot say which strategy will be the best for efficiently simulating PEMFC and stack models. From a mathematical/numerical point of view, novel mathematical methods and innovative numerical schemes will continuously be ameliorated and implemented in CFD software, and add-on modules are often used for PEMFC modeling. Enhanced discretization tools will lead to more efficient meshes, producing a better quality result while lowering the number of cells (e.g., polyhedral mesh).

### 3.2.2 Two-Phase Modeling for Water Management

The two-phase flow in PEMFCs is a unique multiphase flow that occurs due to several factors such as large gas to liquid ratios, the water produced by electrochemical reaction, and water condensing in the flow channels from humidified reactants and other operating conditions. Another important distinction is that water is introduced into the air flow-field channels from a porous GDL instead of each phase being introduced together via a common inlet. Furthermore, the coupled gas and liquid flow rates (via Faraday's law) and the contact angles of each wall (flow-field walls and GDL in the same channel) make two-phase flow studies in PEMFCs a challenge. Liquid water in flow channels can cause channel blockage, which can increase the pressure drop in the channel and result in the formation of a liquid film on the GDL surface, which blocks the reactant gas from reaching active catalyst sites. Experiments have documented the following flow patterns in parallel cathode flow-field channels: slug, film, corner, and mist flow. Film flow is considered a desirable flow pattern for water removal in fuel cells due to water traveling on the sidewalls instead of on the GDL surface. However, a specific combination of surface properties and superficial gas and liquid velocities must be met in order to ensure the desired pattern. Parallel channels have shown to have the potential for high performance when no flooding occurs, but this flow-field configuration is flooding prone, and more research is needed for improved water management.

CFD has been used extensively to model multiphase flow in the gas channels of PEMFCs. Multiphase flow through the cathode side of an interdigitated flow-field was studied using a multi-fluid model [146]. The model employs the so-called multi-fluid approach, which solves one complete set of transport equations for each

phase. The physics of phase change has now been implemented, and the model also accounts for the Kelvin effect. In the interdigitated design, more water was found to be carried out of the cell in the vapor phase compared to the straight channel design, indicating that liquid water management might be less problematic. This effect also leads to the finding that, in the interdigitated design, more waste heat is carried out of the cell in the form of latent heat, which reduces the load on the coolant. Simulation of a fuel cell stack is performed by applying a general numerical model with the Volume of Fluid (VOF) method that was successfully applied to the single PEMFC model to investigate the fluid dynamics, mass transport, flooding phenomenon, and the effects of liquid water on the stack performance [147]. The performance of three single cells in series connection in the fuel cell stack was examined according to the presence of liquid water in different single cells. The distributions of fluid flow, species concentration and the current density were presented to illustrate the effects of liquid water on the performance of each single cell. The numerical results show that the low distribution of species in the flooding cell certainly degrades the performance of this cell. Using the multiphase free-energy lattice Boltzmann method (LBM), the formation of a water droplet was simulated emerging through a micro-pore on the hydrophobic GDL surface in a PEMFC and its subsequent movement on the GDL surface under gas shear stresses [148]. The results showed that water droplet removal was facilitated by high gas flow velocity on a more hydrophobic GDL surface. A highly hydrophobic surface was shown found to be capable of lifting the water droplet from the GDL surface, resulting in the availability of more GDL surface for the transport of gas reactant. A Multiphase-Mixture (M2)-based model was developed for two-phase flow computations in the cathode channels of a PEMFC [149]. Because in a real PEMFC stack, geometry is very difficult to achieve and hence the model has been extended to non-orthogonal hexahedral and tetrahedral meshes, which can be used to mesh any three-dimensional geometry. Additionally, in order to reduce the meshing effort, an immersed body approach has been tested successfully on this model. The resulting two-phase flow model that is valid for arbitrary flow-field geometries is fast and accurate.

The pressure drop hysteresis is a recently studied two-phase flow phenomenon. This behavior occurs when the gas and liquid flow rates (determined by a given current density) are increased along a set path and then decreased along the same path with differing pressure drops. Two-phase flow pressure drop hysteresis was studied in a nonoperational PEMFC to understand the effect of stoichiometry, GDL characteristics, operating range and initial conditions (dry vs. flooded) for flow conditions typical of an operating fuel cell [150]. This hysteresis is noted when the air and water flow rates are increased and then decreased along the same path, exhibiting different pressure drops. The hysteresis was found to be greater when water breakthrough occurs at higher simulated current densities. The operating range had to reach a critical simulated current density between the ascending and descending approach in order to create a pressure drop hysteresis zone. Two-phase flow pressure drop hysteresis was studied in an operating PEMFC. The variables studied include air stoichiometry (1.5, 2, 3 and 4), temperature (50, 75, and 90 °C),

and the inclusion of a microporous layer [151]. The cathode channel pressure drops can differ in PEMFCs when the current density is increased along a path and then decreased along the same path (pressure drop hysteresis). The results showed that the hysteresis occurs with or without the inclusion of a microporous layer.

In terms of fuel and oxidant delivery schemes, DMFCs can be categorized into active-feed DMFCs and passive-feed DMFCs. In passive DMFCs, fuel and oxidant are passively delivered without any moving parts such as pumps, fans, or blowers. A two-dimensional, two-phase, non-isothermal model was developed to investigate the water transport characteristics in a passive liquid-feed DMFC. The two-phase mass transports of liquid–gas in the porous anode and cathode were formulated based on a multi-fluid model in porous media. Moreover, water and methanol crossover through the membrane were considered with the effects of diffusion, electro-osmotic drag, and convection [152]. The results showed that for the free-breathing cathode, gas species concentration and temperature showed evident differences between the cell and the ambient air. The use of a hydrophobic air filter layer at the cathode helped to achieve water recovery from the cathode to the anode, although the oxygen transport resistance was increased to some extent. It was further revealed that the water transport can be influenced by the ambient relative humidity. A one-dimensional, steady-state, two-phase DMFC model was developed to precisely investigate the complex physiochemical phenomena inside DMFCs [153]. The developed model was validated against readily available experimental data in the literature. Next, a parametric study was carried out to investigate the effects of the operating temperature; methanol feed concentration, and properties of the backing layer. The results of the numerical simulation clarify the detailed influence of these key designs and operating parameters on the methanol crossover rate as well as on cell performance and efficiency. The results emphasize that the material properties and design of the anode backing layer play a critical role in the use of highly concentrated methanol fuel in DMFCs.

### 3.2.3 Complex Flow-field Interaction Modeling

In the literature, many models have been developed to take into consideration multi-physical phenomena in PEMFCs. A sequential approach was developed to study the pressure effects by combining the mechanical and electrochemical phenomena in fuel cells [154]. In this research, the pressure causes the deformation of the GDL and impacts the mass transfer and the electrical contact resistance. The GDL porosity in the PEMFC was also affected by the clamping pressure; therefore, a global value of GDL porosity was taken into account (not a local porosity distribution. There is an optimal width of the rib of the bipolar plate that gives a small amount of contact resistance and a good porosity of the GDL. At the same time, the effect of the clamping force on the performance of PEMFCs was investigated with interdigitated gas distributors considering the interfacial contact resistance, the nonuniform porosity distribution of the GDL and the GDL deformation [155]. The clamping force between the GDL and the bipolar plate is one of

the important factors that affect the performance and efficiency of the fuel cell system. It directly affects the structure deformation of the GDL and the interfacial contact electrical resistance, and in turn influences the reactant transport and the Ohmic overpotential in the GDL. The finite element method and the finite volume method were used, respectively, to study the elastic deformation of the GDL and the mass transport of the reactants and products. An optimal clamping force was found to exist for obtaining the highest power density for the PEMFC with the interdigitated gas distributors. The effects of mechanical solicitations were studied on the performance of a PEMFC, as was the coupling between the physicochemical phenomena and the mechanical behavior. A finite element method was first developed to analyze the local porosity distribution and the local permeability distribution inside the gas diffusion layer induced by different pressures applied on deformable graphite or steel bipolar plates [156]. Taking into account the chemical phenomena and the effects of the mechanical compression of the fuel cell to examine a multi-physical approach was carried out to more precisely the deformation of the gas diffusion layer, the changes in the physical properties and the mass transfer in the gas diffusion layer. The effects of varying porosity and permeability fields on the polarization as well as on the power density curves were reported, and the local current density was also investigated. Unlike other studies, this model accounts for a porosity field that varies locally in order to correctly simulate the effect of inhomogeneous compression in the cell.

On the other hand, a computational fuel cell dynamics model was presented in order to elucidate the three-dimensional interactions between mass transport and electrochemical kinetics in PEMFCs with straight and interdigitated flow-fields, respectively [157]. This model features a detailed MEA submodel in which water transport through the membrane with spatially variable transport properties along with spatial variations of the reaction rate and the ionic resistance through the catalyst layer are accounted for. Emphasis was on understanding the way three-dimensional flow and transport phenomena in the air cathode impact the electrochemical process in both types of flow-fields. Fully three-dimensional results of the flow structure, species profiles, and current distribution were presented for PEMFCs with an interdigitated cathode flow-field. The model results indicated that forced convection induced by the interdigitated flow-field substantially improves mass transport of oxygen to, and water removal from, the catalyst layer, thus leading to a higher mass transport limiting current density as compared to that of the straight flow-field. The effects of nonuniform compression of the GDL and GDL intrusion into a channel due to the channel/rib structure of the flow-field plate were investigated numerically [158]. The focus was placed on accurately predicting two-phase transport between the compressed GDL near the ribs and the uncompressed GDL near the channels and on understanding its associated effects on cell performance. A GDL compression model was newly developed and incorporated into the comprehensive, three-dimensional, two-phase PEMFC model developed earlier. To assess the effects of GDL compression and intrusion in isolation, the new fuel cell model was applied to simple single straight channel fuel cell geometry. Numerical simulations with different levels of GDL compression and intrusion were

carried out, and simulation results revealed that GDL compression and intrusion considerably increase the nonuniformity—particularly the in-plane gradient in liquid saturation, oxygen concentration, membrane water content, and current density profiles—which in turn resulted in significant ohmic and concentration polarizations. The three-dimensional GDL compression model yields realistic species profiles and cell performance that help to identify the optimal MEA, gasket, and flow channel designs in PEMFCs.

## *3.3 Validation of Experimental and Numerical Results*

The wide range in power output implies a variation of fuel cell operating conditions, active area, gas diffusion media, bipolar plate, and MEA properties. Therefore, the performance of a PEMFC stack varies significantly with respect to the number of cells, operating conditions, material properties, and flow-field characteristics. The design principles of PEMFC stacks were established for portable applications [97]. A combination of experiments and numerical simulations was used to enhance our understanding of the behavior of this portable PEMFC stack. A three-dimensional CFD-based methodology was utilized to make predictions about the current and temperature distributions of this portable PEMFC stack. The results explained how the baseline operation and original design of this stack impact the local temperature, water content, water transport, and kinetic variables inside the individual cells.

In developing the flow-field design, CFD simulation, experimental test and in situ multichannel impedance analysis were performed in order to optimize the serpentine channel design for a 300-$cm^2$ active area PEMFC stack [159]. The CFD simulation results successfully predicted the channel variation effect on the performance, showing the same trend as that of the experimental test. In situ multichannel impedance analysis not only successfully predicted the experimental result but also explained the performance of each channel within the heterogeneous stack. The experiments carried out in this study also proved that the in situ multichannel impedance analysis with a heterogeneous channel stack is very effective in predicting the channel performance and analyzing the reasons behind the difference in the performance between channels. Finally, it was shown that in situ multichannel impedance has the advantages of reducing the analysis time and gathering synchronous data from several cells. The operating characteristics of 5 W class DMFC stacks, using the flow-field patterns of serpentine, parallel, and square spot, were investigated to compare how capable these characteristics are with mass transport and water removal in the cathode [160]. The stability of the stack was predicted through the simulation results of the flow-field patterns on the pressure drop and the water mass fraction in the cathode of the stack. It was then estimated through the performance and the voltage distribution of the stack. According to the simulation results, although the square spot pattern shows the lowest pressure drop, the square spot pattern had a much higher water mass fraction in the central region of the channel compared to the other flow-field patterns.

The flow-field structures can exert a significant influence on both flow velocity and temperature distributions of the DMFCs. Thus, proper flow-field constructions are very important for the improvement of the DMFC's performance. Anodic flow velocity and temperature distributions based on four different designs, including double serpentine, parallel, helix, and single serpentine have been simulated in three-dimensional models [161]. Computational fluid dynamics was used to investigate the effects of flow-field structures on the DMFC's performance. Simulated results indicated that the double-serpentine flow-field showed better flow velocity distribution and more uniform temperature distribution, which might be helpful for better performance of the DMFC. Further experimental investigation of four types of flow-fields also confirmed that the DMFC with a double-serpentine flow-field structure exhibited a maximal power density at a variety of inlet velocities, which was in good agreement with the simulated results. The CFD simulations showed that the initial solution of the fuel cell model developed for a 50-$cm^2$ PEMFC with parallel and serpentine flow-fields was not fully converged in the mass transport polarization region for a particular case and therefore the flow-field did not reach a steady-state solution [162]. This point is especially critical for the multiphase flow variables, as these are generally difficult to converge. An increase in the under-relaxation factors resulted in a better convergence with a fully developed flow-field, and also worked best for the multiphase-related variables. The polarization curve predicted by the CFD model showed better accuracy compared with the experimental data once the fully converged solution was achieved. Enhanced convergence controls for PEMFC CFD simulations are still needed, such as the monitoring of the variation of water content and water saturation in both CL and GDL. These enhanced controls will ensure that further modifications in the solver parameters do not modify the flow-field, especially for the multiphase-related variables.

## 4 New Flow-field Optimization Approaches Utilizing Under-Rib Convection

In principle, the channel structure offers a homogeneous flow distribution with low-pressure drops. But, on the other hand, the formation of liquid water droplets at the cathode can flood one or more channels with the consequence of stopping the gas flow there. In order to effectively utilize the area, flow distribution should be as homogeneous as possible. In addition, pressure losses should be minimized with regard to the power demand of auxiliary components such as pumps and compressors. In PEMFCs and DMFCs, the flow-field is in direct contact with the diffusion layer. The main task of the diffusion layer is to distribute the reactants from the flow-field toward the catalyst layer. The diffusion layer is general highly porous and provides high reactant fluxes to prevent diffusion overvoltage. Consequently, the flow distribution in the flow-field can be superpositioned by a

flow in the diffusion layer. The interaction between the diffusion layer and the flow-field has been experimentally examined for DMFC [5]. To avoid depletion of reactants in specific regions of the cell, the geometry of the meander should be chosen with regard to the permeability of the diffusion layers. Unsuitable combinations of meander geometry and diffusion layer properties lead to even lower flow homogeneities compared to the flow passing only in the diffusion layer. High permeabilities require meander structures with low-pressure losses; otherwise, the flow homogeneity decreases. Additional simulation studies will help in understanding these processes and to determine suitable combinations of flow-fields and diffusion layers.

The presence of a convective flow in the under-rib regions enables more effective utilization of electrocatalysts by increasing reactant concentrations and facilitating liquid water removal in those regions [32]. The mechanism of under-rib convection was explained with three neighboring channel regions A, B, and C in the exemplary serpentine flow-field shown in Fig. 10a. The path-lengths $Z_A$, $Z_B$, and $Z_C$ are defined as the distances traveled by the reactants from an inlet to the three regions along the channel as illustrated by the dotted lines in Fig. 10a. The path-length, $z$, can be viewed as a coordinate whose upper limit is the same as the total length of the path, $z_{max}$. The pressure and the reactant concentration in PEMFCs are expected to change linearly along the flow channel, i.e., with respect to $z$. The total flow rate, $q_{tot}$, depends on the total pressure drop, $\Delta p_{tot}$, across the flow-field expressed as follows:

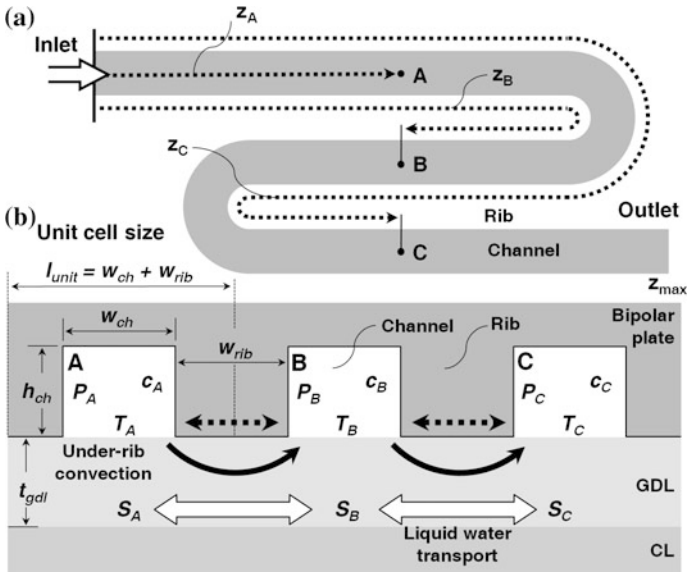


**Fig. 10** Under-rib convection and transport in serpentine flow-field: **a** definition of path-length, $z$; **b** under-rib convection and transport mechanisms. *Source* Ref. [32]

$$q_{\text{tot}} = \frac{K_{\text{ch}}}{\mu} A_{\text{ch}} \frac{\Delta p_{\text{tot}}}{Z_{\max}} \tag{1}$$

where $\mu$ is the viscosity, $A_{\text{ch}}$ is the cross-sectional area of the channel (height $h_{\text{ch}} \times$ width $w_{\text{ch}}$), and $K_{\text{ch}}$ is the channel permeability derived from the Hagen–Poiseuille equation. Note that Eq. (1) assumes that the flow rate is constant along the channel with a low under-rib convection flow rate ($q_{\text{rib}} \approx 0$) and that the secondary (nonlinear) pressure loss in 90° or 180° corners is negligible. The pressure difference between two neighboring channel regions is expressed in terms of the path-length difference as:

$$|p_{\text{A}} - p_{\text{B}}| = \frac{\Delta p_{\text{tot}}}{Z_{\max}} |z_{\text{A}} - z_{\text{B}}| \tag{2}$$

Let us assume that the flow-field shown in Fig. 10a is for the cathode of a PEMFC. The reactant concentration, $c$ (mol/m$^3$), then denotes the molar concentration of oxygen, and the total concentration loss across the flow-field, $\Delta c_{\text{tot}} = c_{\text{in}} - c_{\text{out}}$, is calculated from the mass balance of oxygen according to:

$$(c_{\text{in}} - c_{\text{out}}) q_{\text{tot}} = \Delta c_{\text{tot}} q_{\text{tot}} = \frac{I_{\text{tot}}}{4F} \tag{3}$$

Here, $I_{\text{tot}}$ (A) is the current generated over the entire cell area and $F$ is the Faraday constant (96,487 Cmol$^{-1}$). Note that Eq. (3) ignores the change in the total flow rate, $q_{\text{tot}}$, due to oxygen consumption. In fact, the reactant flow rate in the cathode vicinity is relatively constant because the humidified air is supplied at high excess air ratios. If current is generated uniformly throughout the active area, the concentration difference between two neighboring channel regions is also expressed in terms of the path-length difference, i.e.:

$$|c_{\text{A}} - c_{\text{B}}| = \frac{\Delta c_{\text{tot}}}{z_{\max}} |z_{\text{A}} - z_{\text{B}}| = \frac{I_{\text{tot}}}{4F q_{\text{tot}} z_{\max}} |z_{\text{A}} - z_{\text{B}}| \tag{4}$$

Figure 10b shows the cross-sectional view of the three adjacent channel regions (A, B, and C). Region A has the highest pressure and reactant concentration, whereas region C has the lowest of the three regions ($p_{\text{A}} > p_{\text{B}} > p_{\text{C}}$ and $c_{\text{A}} > c_{\text{B}} > c_{\text{C}}$). Due to the pressure difference between neighboring regions, convective flow occurs through under-rib regions in the GDL, as shown in Fig. 10b. This additional convective flow through GDLs is called the under-rib convection and is believed to improve the performance of PEMFCs. Under-rib convection increases the reactant concentration in the under-rib regions, facilitates liquid water removal from those regions, and enables a more uniform concentration distribution throughout the flow-fields. The under-rib convection flow rate, $q_{\text{rib}}$, is proportional to the pressure difference between two neighboring regions. For example, $q_{\text{AB}}$ rib between regions A and B in Fig. 15b can be expressed as:

$$q_{\mathrm{rib}}^{\mathrm{AB}} = \frac{K_{\mathrm{gdl}}}{\mu} A_{\mathrm{rib}}^{\mathrm{AB}} \frac{|p_{\mathrm{A}} - p_{\mathrm{B}}|}{w_{\mathrm{rib}}} = q_{\mathrm{tot}} \frac{K_{\mathrm{gdl}} A_{\mathrm{rib}}}{K_{\mathrm{ch}} A_{\mathrm{ch}}} \frac{|z_{\mathrm{A}} - z_{\mathrm{B}}|}{w_{\mathrm{rib}}} \tag{5}$$

where $K_{\mathrm{gdl}}$ is the flow permeability of the GDL, $w_{\mathrm{rib}}$ is the rib width, and $A_{\mathrm{rib}}^{\mathrm{AB}}$ is the flow area for the under-rib convection. Note that $A_{\mathrm{rib}}^{\mathrm{AB}}$ is determined by multiplying the GDL thickness, $t_{\mathrm{gdl}}$, together with some length, $l_{\mathrm{ch}}$, of the regions along the channel (the under-rib convection through the catalyst layer is ignored).

Figure 10b shows that other transport mechanisms also become operative when channel regions that have different path-lengths are in close contact. The local temperature and liquid water saturation in GDLs depend on the electrochemical reaction rate, and this rate is generally governed by the reactant concentration, which varies along the channel (with respect to $z$). The temperature gradient due to closely placed channels of different path-lengths facilitates conductive heat transfer by the under-rib or cross-rib paths, and the water saturation gradient facilitates the capillary transport of water by the under-rib path. These transport mechanisms may be termed as under-rib transports to distinguish them from under-rib convection. Whereas under-rib convection occurs in only one direction (from a high-pressure region to a low-pressure region), under-rib transport may occur in both directions, as shown in Fig. 10b. In fact, the successful dry operation of a PEMFC was attributed to the under-rib transport of water in the opposite direction of the under-rib convection [163].

In the following, new flow-field approaches by the above-stated under-rib convection aim to enhance the uniformity of operative conditions in the flow-fields, including the reactant and product concentrations, temperature and liquid water saturation. The flow-field pattern that activates the internal mass transfer mechanism of PEMFCs is able to improve its performance from a mechanical engineering perspective. In other words, this mechanical method can improve the performance of the fuel cells without changing the electrochemical materials. The promotional role of under-rib convection is (a) to provide a homogeneous distribution of the reactants, (b) ensure the uniformity of temperature and current distributions, (c) facilitate liquid water discharge, (d) reduce the pressure drop and parasitic losses, and (e) improve cell output power. These studies are listed schematically in Table 1 and are described in this section in order to provide guidance to the optimization of flow-field design by under-rib convection.

## *4.1 Homogeneous Distribution of the Reactants*

In a PEMFC, anode and cathode gases usually flow through each channel, and the reactant gas diffuses to the interface of MEA through GDL. GDL is porous, and it plays a role in helping hydrogen and oxygen to move to the electrode catalyst, in order to support MEA and to pass the electron. However, in the case of a large-scale cell, the differential pressure between adjoining channels is thought to increase,

**Table 1** Experimental and numerical studies on under-rib convection used in this article

| Flow-field details | PEFC types | Experiment/Simulation | Features | Refs. |
|---|---|---|---|---|
| 100 $cm^2$ meander structure | PEMFC/DMFC | Experiment/Simulation | Flow interaction between the diffusion layer and the flow-field, validation of experiments using DMFC cells | [5] |
| Parallel mini-channels | PEMFC | Experiment | Flow maldistribution and flow hysteresis of gas and liquid two-phase flow, presence of gas shorting between channels | [9] |
| Square serpentine channels | PEMFC | Simulation | Convective transport as a function of GDL permeability | [10] |
| 25 $cm^2$ serpentine, parallel, semi-serpentine separator | PEMFC | Simulation | Effect of gas channel depth on current density distribution using oxygen transfer and thermal flow analysis models | [11] |
| 20 straight channels connected in a serpentine fashion | PEMFC | Simulation | Three-dimensional flow and mass transfer model, water transport by both electro-osmosis and diffusion processes | [12] |
| Parallel flow-field | PEMFC/DMFC | Experiment/simulation | Inefficient usage of the electrochemically active area due to poor water management | [13] |
| Single serpentine flow-field | PEMFC | Experiment | Convection contributes to the limiting current. | [14] |
| Serpentine flow channels with a square cross-section | PEMFC | Simulation | The effect of channel-to-channel gas crossover on the pressure and temperature distribution | [15] |
| Serpentine channel system | PEMFC | Simulation | Pressure distribution and flow crossover through the GDL | [16] |
| Serpentine/parallel flow-fields | PEMFC | Simulation | Significant cross-flow can lead to more effective evacuation of the water vapor | [17] |
| Serpentine flow-fields | PEMFC/DMFC | Experiment/simulation | An increase in power density by optimal use of the cross convection effect | [18] |
| Flow-field parameters | PEMFC | Simulation | The extent of reactant bypass through the GDL from one channel to the other enhances reaction rates | [19] |
| Double-path serpentine with 36 channels | PEMFC | Simulation | Provides a unique opportunity to explore the rich physics behind the complex flow and transport phenomena | [20] |
| Serpentine flow channels | PEMFC | Simulation | Cross-leakage flow can help in the reduction of overpotential and the effective removal of liquid water | [21] |

(continued)

**Table 1** (continued)

| Flow-field details | PEFC types | Experiment/Simulation | Features | Refs. |
|---|---|---|---|---|
| Single serpentine flow-field | PEMFC | Simulation | Convective bypass can be increased by simply increasing the length of the flow channel | [22] |
| Flow-field parameters | DMFC | Experiment | The reduced cell performance, as a result of thinning the backing layer, may be attributed mainly to the increased under-rib mass transport polarization | [23] |
| Serpentine flow channel | PEMFC | Experiment/simulation | Cross-flow through the gas diffusion layer between the adjacent flow channels helps drive the liquid water | [24] |
| 50, 100, 200, 300, and 441 $cm^2$ serpentine flow channels | PEMFC | Experiment/simulation | The effectiveness in water removal is confirmed by two different experimental observations | [25] |
| Simple straight channel | PEMFC | Simulation | Thoughts on which combination of geometric design parameters would be optimal to get the best performance | [26] |
| Single serpentine flow-field | DMFC | Experiment/simulation | Under-rib convection plays an important role in making the reactant evenly distributed over the entire catalyst layer | [23] |
| Serpentine/parallel flow-fields | DMFC | Experiment/simulation | The overall methanol-transfer coefficient can be significantly increased due to the enhanced under-rib convection | [27] |
| Convection-enhanced serpentine flow-field | PEMFC/DMFC | Experiment/simulation | Multiple serpentines in parallel do not lose under-rib convection and result in a smaller pressure drop | [28] |
| Novel serpentine-baffle flow-field | PEMFC | Simulation | The baffled design increases the limiting current density and improves the cell performance relative to conventional design | [29] |
| Single serpentine flow-field | PEMFC | Simulation | Reduced channel heights enhance sub-rib convection to transport oxygen to and liquid water out of the diffusion layer | [30] |
| Single serpentine flow-field | DMFC | Experiment/simulation | A comparison of the influence of two-phase flow and under-rib mass transfer on DMFC performance | [31] |
| Multi-pass serpentine flow-fields | PEMFC | Simulation | Multi-pass serpentine flow-fields lead to significantly higher under-rib convection intensities | [32] |

(continued)

**Table 1** (continued)

| Flow-field details | PEFC types | Experiment/Simulation | Features | Refs. |
|---|---|---|---|---|
| Single and triple serpentine flow-fields | PEMFC | Simulation | The sub-rib convection is much higher for single serpentine flow than the triple serpentine flow cells | [33] |
| Parallel/interdigitated/serpentine flow-fields | PEMFC | Simulation | Flow design that enhances cell performance also increases pressure drop over a working PEMFC | [34] |
| Single serpentine flow-field | PEMFC | Simulation | The role of sub-rib convection on cell performance and optimization of the cathode flow-field design | [35] |
| New tapered single serpentine flow-field | DMFC | Simulation | Tapered flow-field enhances the pressure difference between the adjacent flow channels and improves mass transport efficiency | [36] |
| 1/3/5 parallel path serpentine flow-fields | PEMFC | Simulation | Enhanced under-rib convection intensity was the key reason for the performance enhancement | [37] |
| Parallel/interdigitated flow-fields | PEMFC | Simulation | The effect of the channel to rib width ratio on the transient characteristics of the parallel but less on the interdigitated fields | [38] |
| Tapered flow channel installed with a baffle plate | PEMFC | Simulation | The tapered flow channel with a baffle plate enhances the overall cell performance | [39] |
| Split serpentine flow-field | PEMFC/DMFC | Experiment/simulation | The splitting of the channel with enhanced cross-flow in selected regions more prone to localized flooding | [40] |
| Serpentine flow channel | PEMFC | Simulation | The findings make it possible to optimize the design of gas flow channels for a more efficient PEMFC | [41] |
| Serpentine flow-field with sub-channels/by-passes | PEMFC | Experiment/simulation | The flow-field pattern that activates the internal mass transfer mechanism can improve its power density from a mechanical engineering perspective | [42] |

allowing the supplied gas to flow through GDL. As a result, the cell endurance is assumed to decrease because the temperature and the humidity conditions are not uniform. However, the oxygen transfer rate to the electrode and the output density can be expected to increase via such gas flow in the GDL. Therefore, it is important to examine the influence of this gas flow on cell performance and to optimize operating conditions and cell shape [11]. Cell areas supplied with low amounts of reactants are affected by diffusion overvoltages in the electrodes, which lower the current density. Below, the parameters characterizing the flow homogeneity are defined.

In a system consisting of a meander structure and a diffusion layer, there are two borderline cases. The first assumes low permeabilities of the diffusion layer. In this case, the overall flow is guided through the meander only. The second borderline case describes a high permeability of the diffusion layer compared to that of the meander. This case results in the total flow passing through the diffusion layer. The mean specific volume flow $\overline{\dot{v}}_{\mathrm{spec}}$ is equivalent to the inlet volume flow $\dot{V}$ divided by the cell area $A_{\mathrm{cell}}$. This parameter will be used for the calculation of the flow homogeneity by comparison with the local flow rates. By integrating the local volume flow $\dot{V}_{\mathrm{local}}^{\mathrm{meander}}$ (l/h) over the entire length of the meander channel $L_{\mathrm{M}}$, the specific volume flow in the meander channel $\overline{\dot{v}}_{\mathrm{spec}}^{\mathrm{meander}}$ is obtained as

$$\overline{\dot{v}}_{\mathrm{spec}}^{\mathrm{meander}} = \frac{1}{A_{\mathrm{cell}}} \frac{1}{L_{\mathrm{M}}} \int_0^{L_{\mathrm{M}}} \dot{V}_{\mathrm{local}}^{\mathrm{meander}} \mathrm{d}L_{\mathrm{M}} \tag{6}$$

The flow cross-section in the inlet or the outlet is substantially smaller than that in the middle of the cell. The total specific flow through the diffusion layer $\overline{\dot{v}}_{\mathrm{spec}}^{\mathrm{diff}}$ is obtained by mass conservation:

$$\overline{\dot{v}}_{\mathrm{spec}}^{\mathrm{diff}} = \overline{\dot{v}}_{\mathrm{spec}} - \overline{\dot{v}}_{\mathrm{spec}}^{\mathrm{meander}} \tag{7}$$

The overall flow homogeneity $\psi$ results in

$$\psi = \left( \frac{\overline{\dot{v}}_{\mathrm{spec}}^{\mathrm{meander}}}{\overline{\dot{v}}_{\mathrm{spec}}} \right)^2 - \frac{1}{2} \left( \frac{\overline{\dot{v}}_{\mathrm{spec}}^{\mathrm{diff}}}{\overline{\dot{v}}_{\mathrm{spec}}} \right)^2 \tag{8}$$

This equation is a semiempirical expression valid for a meander flow-field combined with a porous diffusion layer [5]. Of course, if the bipolar plate itself is porous, such as porous carbon materials with a meander structure manufactured inside, then the resulting flow can be described equivalently. The influence of the permeability of the diffusion layer for four different cell geometries using the simulation is summarized in Fig. 11. The flow homogeneity $\psi$ was calculated according to Eq. (8). The thickness of the diffusion layer was assumed to be

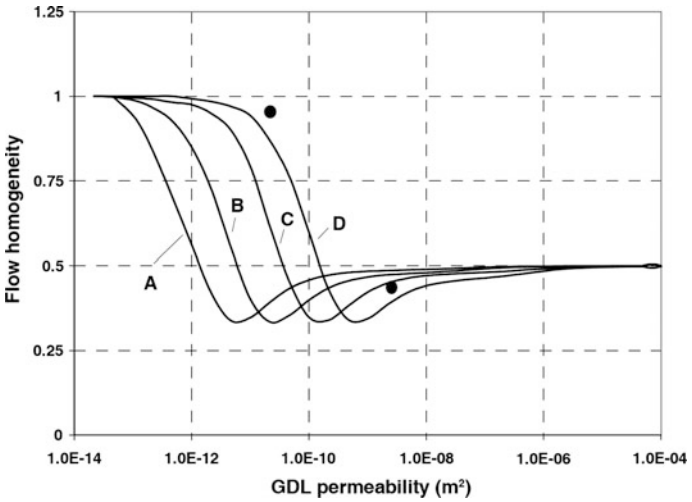


**Fig. 11** Influence of the permeability of the diffusion layer on the flow homogeneity for different cell geometries. Results based on simulation. The *dots* represent the correlation with the experimentally tested flow-field geometries. *A* Cell area 200 mm × 200 mm, meander cross-section 1 mm × 1 mm. *B* Cell area 100 mm × 100 mm, meander cross-section 1 mm × 1 mm. *C* Cell area 200 mm × 200 mm, meander cross-section 2 mm × 2 mm. *D* Cell area 100 mm × 100 mm, meander cross-section 2 mm × 2 mm. *Source* Ref. [5]

0.4 mm in all cases. Flow homogeneity helps to evaluate different flow-fields, but it is not the sole criterion for the evaluation of flow-fields or for the decision regarding whether or not a flow-field is suitable. Another important parameter, especially for the cathode of fuel cells, is the pressure drop that requires compressor work and thus reduces the total system power. In general, a flow-field is a compromise between flow homogeneity and a low-pressure drop. In our simulation studies, the pressure drop will also be taken into account.

As shown in Fig. 12, two 25 $cm^2$ serpentine flow-fields of 5-passes and 4-turns were considered in this study. Through the previous geometrical characterization of serpentine flow channels with various heights and widths, a conventional-advanced serpentine flow-field (CASFF) without sub-channel was selected as a design standard [41]. The presence of under-rib convection enables more effective utilization of electrocatalysts by increasing reactant concentration and facilitating liquid water removal. As shown in Figs. 13b, c and 14b, c, in case of anode side of CASFF, generally uniform velocity vectors can be observed at main channel and rib; however, it shows minor change from the inlet to the outlet direction. In addition, the velocity vectors are significantly increased at the turn rib area due to the large pressure difference between adjacent main channels. Also, in case of cathode side, under-rib convection is generated from the inlet to the outlet direction due to high stoichiometry ratio. And in case of serpentine flow-field with sub-channels and by-passes (SFFSB), rib width is decreased therefore improving gas permeability and overall gas diffusion force as we add sub-channel to change

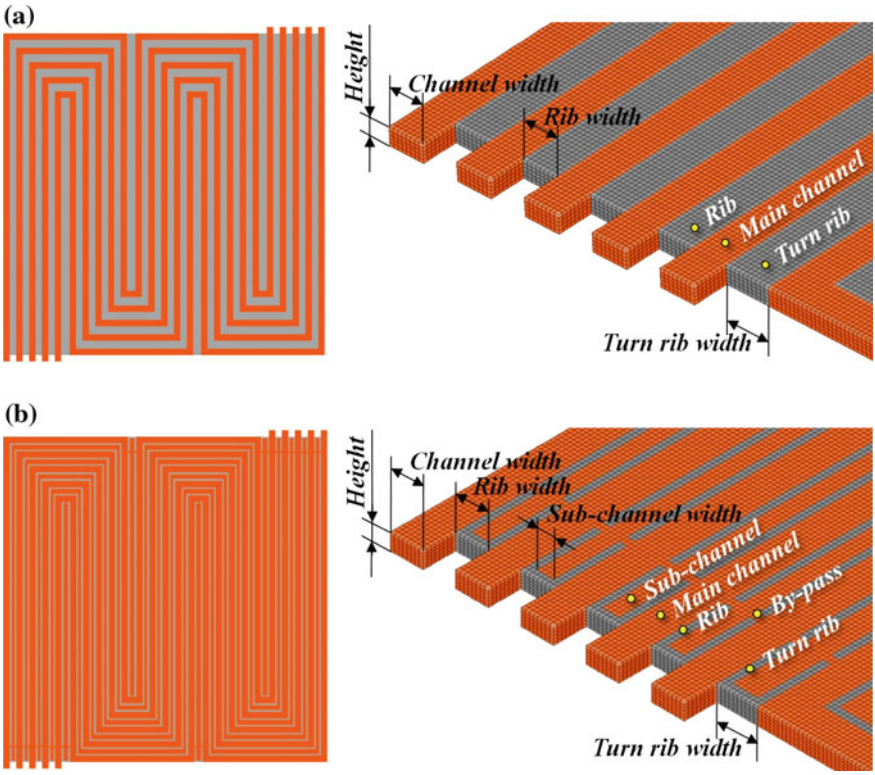


**Fig. 12** Two 25 $cm^2$ serpentine flow-field patterns of 5-passes and 4-turns; **a** conventional-advanced serpentine flow-field (CASFF), **b** serpentine flow-field with sub-channels and by-passes (SFFSB)

the flow direction of under-rib convection. Therefore, in case of anode, the velocity vectors are large at the main channel inlet and under-rib convection flow direction converges to sub-channel through convection because the pressure of main channel is higher than sub-channel. The velocity vectors are uniform the main channel outlet due to the pressure decrease. In case of cathode side, the under-rib convection which has different size but similar tendency with anode side is generated, and the flow direction of the under-rib convection is changed from sub-channel to main channel at the channel outlet due to high stoichiometry ratio. This is because the internal pressure of sub-channel is increased as the reactant which traveled through sub-channel migrates to the outlet, so the flow direction is changed toward the main channel for smooth discharge. Therefore, we can illustrate the representative under-rib convection flow direction and liquid water transport mechanisms of CASFF and SFFSB as shown in Figs. 13a and 14a. From the velocity vectors shown in Figs. 13b, c and 14b, c, numerical analysis result of hydrogen and oxygen mass fractions as well as under-rib convection flow direction can be estimated.

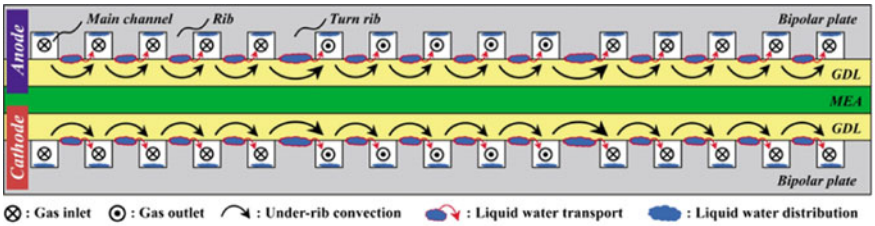


(a) Water behavior with CASFF

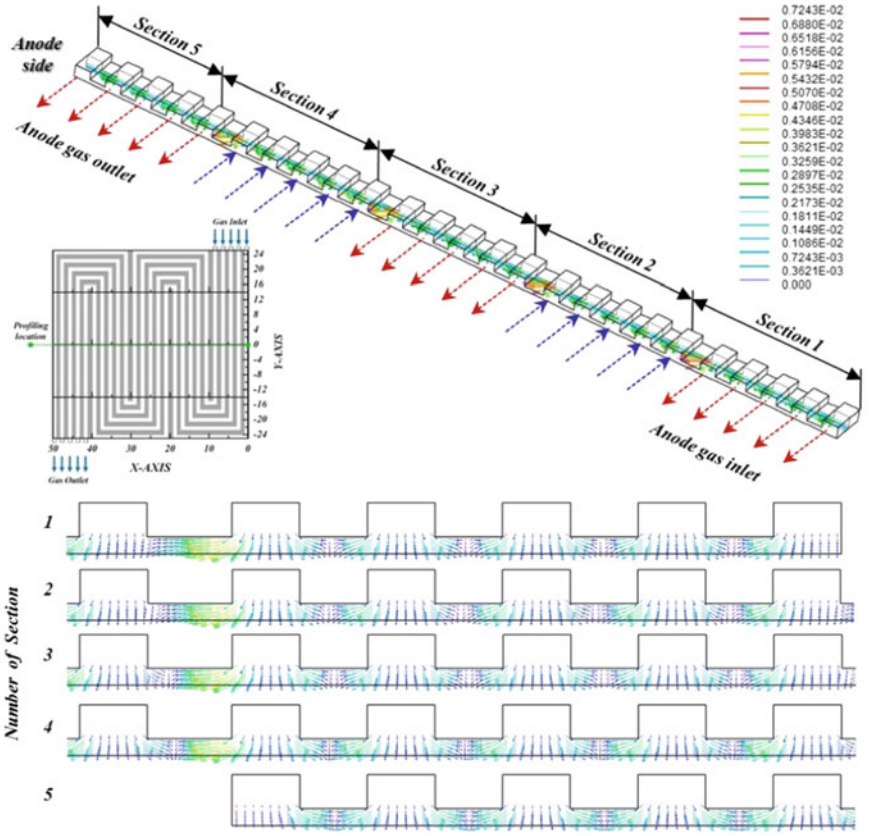


(b) Velocity vectors of anode side with CASFF

**Fig. 13** Cross-sectional views illustrating the under-rib convection and liquid water transport mechanisms and velocity vectors of reactants in the conventional-advanced serpentine flow-field (CASFF) without sub-channel: **a** water behavior; **b** velocity vectors of anode side; **c** velocity vectors of cathode side

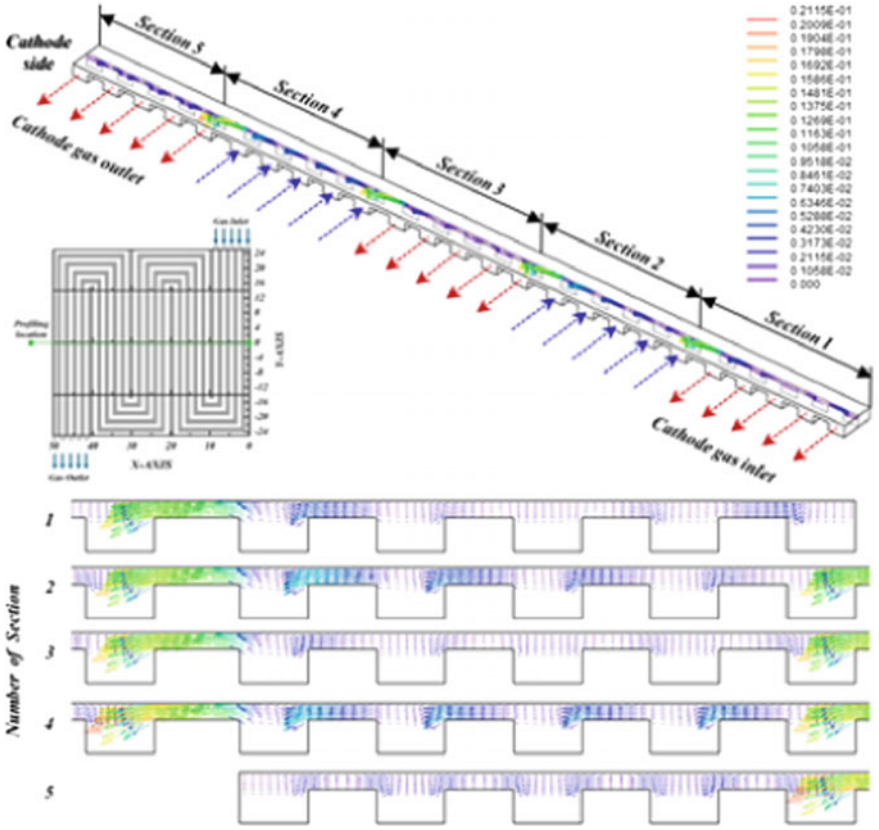


(c) Velocity vectors of anode side with CASFF

**Fig. 13** (continued)

A new flow-field design based on the splitting of the channel with enhanced cross-flow in selected regions has been proposed. Its principal hydrodynamic features were demonstrated using CFD analysis [164]. It could be observed from the vectors heading from the straight section of the serpentine channel towards the U-bends that significant under-rib convection existed from the straight feeder channel into each of the U-bend portions through the GDL. Similar under-rib convection could be observed in all the U-bend regions and in the corresponding straight channels in the three serpentine channels. This cross-flow could also be seen to be higher towards the end channels. This effect on the flow rate through the individual serpentine channels is shown in Fig. 15, where the predicted velocity at mid-channel height and length across various serpentine portions of the three split serpentine channels is shown as a function of distance in the width direction of the flow-field. This contributes in reducing the overall pressure drop and increasing the stoichiometric ratio for the end channels.

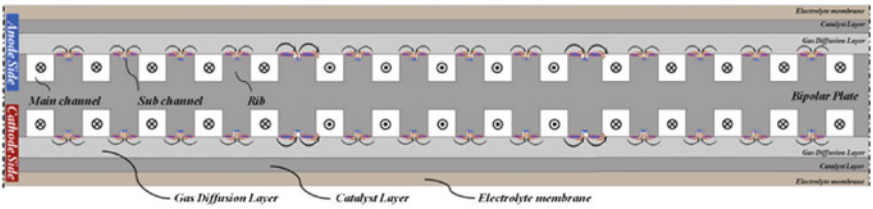


(a) Water behavior with SFFSB

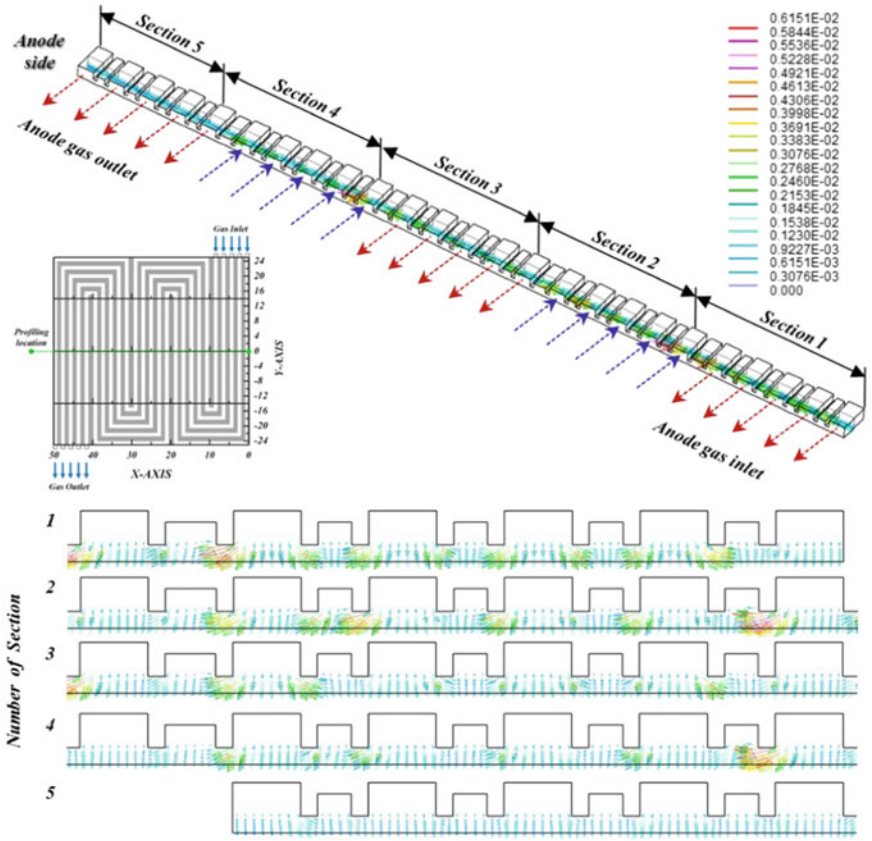


(b) Velocity vectors of anode side with SFFSB

**Fig. 14** Cross-sectional views illustrating the under-rib convection and liquid water transport mechanisms and velocity vectors of reactants in the serpentine flow-field with sub-channels and by-passes (SFFSB) with sub-channel: **a** water behavior; **b** velocity vectors of anode side; **c** velocity vectors of cathode side

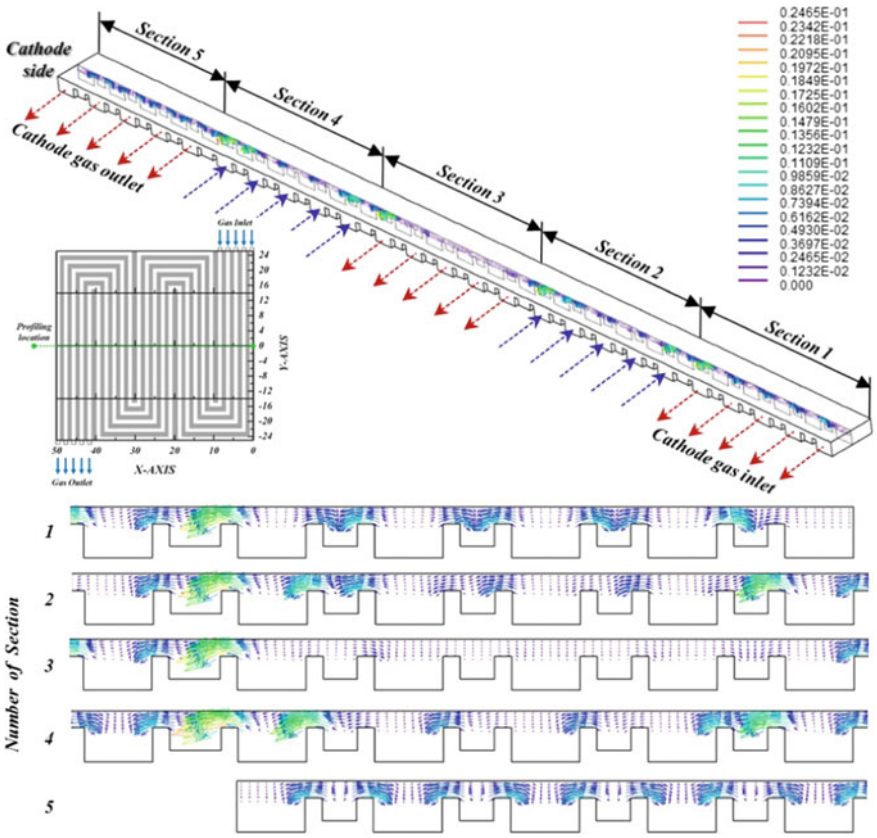


(c) Velocity vectors of anode side with SFFSB

**Fig. 14** (continued)

Methanol crossover is driven by diffusion, electro-osmosis, and convection. These three factors contribute differently under different operating conditions. Nevertheless, all three depend on the local methanol concentration in the PEM. Hence, the maximum crossover flux is expected at the open-circuit voltage where the highest mass transfer of un-reacted methanol occurs. When the current density increases, the excess methanol at the interface between the anode catalyst layer and the PEM decreases. Accordingly, methanol crossover is reduced to almost zero after the current density approaches to its limiting point where nearly all methanol molecules are consumed during electrochemical reaction. This result indicates that diffusion dominates in methanol crossover, except in the region near the limiting current density. In this region, the methanol concentration at the interface of the catalyst layer and the PEM decrease due to the mass transport limitation and high current output.

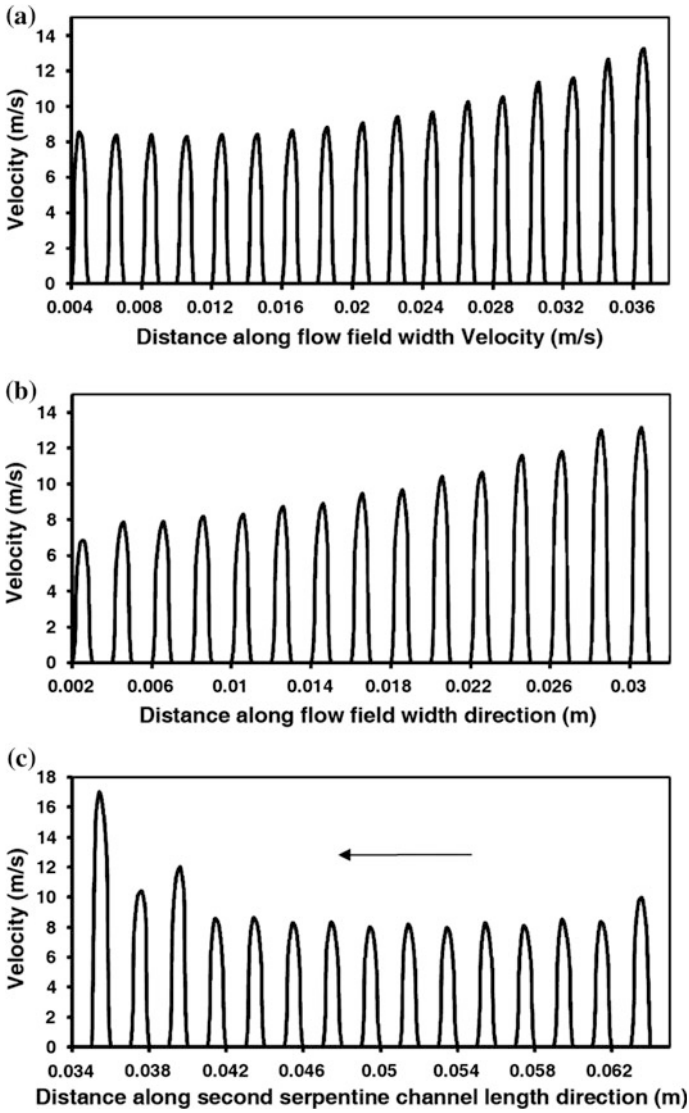


**Fig. 15** Predicted velocity variations at mid-channel height showing the channel-to-channel variation of velocity in the mid-length of **a** first serpentine channel, **b** third serpentine channel and **c** second serpentine channel. *Source* Ref. [40]

Therefore, the diffusion of methanol flux governed by the concentration gradient in the PEM is markedly suppressed. The electro-osmosis drag flux, on the other hand, does not decrease significantly because it is proportional not only to the decrease in methanol concentration but also to the increase in cell current density. Once the current density reaches to its limiting point, the diffuse flux becomes zero because on

the absence of concentration gradient. The electro-osmosis drag flux of methanol also reduces to zero, because there is no methanol content in the electro-osmosis water flux transferring through the membrane.

## 4.2 Uniformity of Temperature and Current Density Distributions

An ideal flow-field design would enable uniform gas mole fractions over the entire surface area of the cell. This ideal design would lead to a uniform distribution of current density and thus produce uniform distributions of temperature and water production. These uniform distributions cause less mechanical stresses on the MEA and lead to longer cell lifetimes. In the real fuel cells, mass transport losses are minimized by employing the intricate flow structures containing many small flow channels. Compared to a single-chamber design, a design that employs many small flow channels keeps the reactants constantly flowing across the fuel cell, facilitating uniform convection and homogeneous distribution. Small flow channel designs also provide more contact points across the surface of the electrode from which the fuel cell electrical current can be harvested. An intricate design promotes forced convection of the reactants through the GDL. This design has been the subject of recent attention because it provides far better water management, leading to an improved mass transport. The problem with the forced convection through the GDL is that it leads to significant pressure drop losses. However, this major disadvantage can be overcome by employing extremely small rib spacing [41].

With an appropriate design of the flow channel of the bipolar plate, designers can enhance the cell performance of a PEMFC system effectively. A projection finite element analysis with an element-by-element preconditioned conjugated-gradient method was used to investigate the non-isothermal tapered flow channel installed with a baffle plate for enhancing cell performance in the cathodic side of a PEMFC [39]. The stronger composite effect of tapered flow and blockage was seen to result in a lower and more uniform temperature distribution in the fuel flow channel. In general, the improvement seen in the single-phase convection heat transfer performance in the fuel flow channel may be caused by an increasing flow interruption, a reduction in the thermal boundary layer, or an increased velocity gradient near the GDL boundary. In order to improve the reduction of the cell performance in the downstream region, a non-isothermal tapered flow-field design was considered to reduce the reflection in the downstream region. The stronger composite effect of the tapered flow channel and baffle blockage results in better performance of convection heat transfer and a higher fuel flow velocity, which in turn improves the local current density and polarization characteristics with a penalty of high-pressure loss.

The PEMFC system consists of many parts, and the bipolar plate is one of the key components. Channels at the bipolar plate distribute air on the cathode side and

hydrogen on the anode side, which are essential for the electric-chemical reaction to produce electricity. Bipolar plates may also be used as a path for the cooling of water to control the temperature of the cell. A parametric study was conducted in order to find the optimal design of the bipolar plate in the PEMFC system for automobiles [26]. First, the design parameters of a bipolar plate are defined. Then, an analysis is conducted on how the combination of those parameters would affect the performance of the fuel cell. Finally, the computation is done for the optimum combination of the parameters. The local current density, concentration and pressure of the reacting gases, cell temperature, and water distribution were obtained by CFD calculation using electrochemical variables fitted by a *V–I* curve from the real system. There is an optimal combination of the design parameters through a trade-off between the performance and the pressure drop in the system design [41].

In order to apply a numerical analysis to design an actual scale separator in PEMFC, the calculation size must be enlarged. Mass transfer and flow in GDL were calculated, and a GDL mass transfer approximate model based on the theoretical model was developed. Next, with this model, a PEMFC reaction and thermal flow analysis model was created. Furthermore, the effects of the separator channel depth on output performance and current density distribution were examined using this numerical analysis [11]. As a result, in the case of shallow channels, the oxygen transfer rate to the electrode increased because of gas flow in GDL. However, current density distribution and pressure drop also increased.

### *4.3 Facilitation of Liquid Water Discharge*

Dynamic water balance and management have imposed one of the dormant technical challenges on PEMFC design and operation, and directly influence the performance and lifetime of PEMFC systems. The importance of the water balance and management arises from the fact that the PEM used in PEMFC requires full hydration in order to maintain good performance and lifetime. The guarantee of membrane hydration under full operating conditions has been achieved, with a good degree of success, by supplying fully humidified reactant gas streams for both the anode and cathode. However, water is produced at the cathode as a result of an electrochemical reaction, and water is also transported from the anode to the cathode through the membrane electrolyte via the electro-osmotic drag effect. Water transport may also occur due to the local gradients of the pressure and/or concentration. Consequently, liquid water flooding occurs if water is not removed adequately from the cell (the cathode in particular). Water flooding will make the PEMFC performance unpredictable, and unrepeatable under nominally identical operating conditions. As a result, elaborate experimental diagnostics and schemes need to be implemented in order to achieve consistent results with much lower performance and limiting current densities [25]. Therefore, water management has become a delicate task; both too much and too little water can adversely impact the performance and lifetime of PEMFCs. Maintaining a perfect water balance during

the dynamic operation process has posed a significant challenge for PEMFC design and operation, and hence water management is a critical issue for PEMFCs.

The design of flow-fields grooved in the bipolar plates of polymer electrolyte membrane fuel cells becomes important at high current densities. Many flow-field designs are being studied to enhance the current density and homogeneity of the reactants in order to overcome the challenges of pressure losses and removal of water from the cathode [22]. One of the features of a serpentine flow-field is the high-pressure drop in the flow direction. This drop creates a significant pressure difference between two neighboring channels that may lead to the under-rib convection. Because the pressure difference across neighboring channels varies along the length, the strength of the cross-flow also varies significantly and is lower in the U-bend region. This variation may cause insufficient evacuation of water vapor in the region and lead to build-up and eventual local flooding. In the present paper, this scenario is verified by means of CFD simulations. This result would indicate that the measures that improve local under-rib convection may lead to a better design of the flow-field. If the electrode permeability or the pressure drop is high, then significant under-rib convection can be established which leads to more effective evacuation of the water vapor. The superior performance of the convection-enhanced serpentine flow-field may also be attributed to this process. Hence, under-rib convection can be used as an additional parameter in arriving at the optimum design of a flow-field [17].

The cathode flow-field design of PEMFC determines its reactant transport rates to the catalyst layer and the removal rates of liquid water from the cell. The cathode flow-field has been optimized for a single serpentine PEM fuel cell with 5 channels using the heights of channels 2–5 as search parameters. An optimization approach that integrates the simplified conjugated-gradient scheme and a three-dimensional, two-phase, non-isothermal fuel cell model has also been described [35]. Because most oxygen at the cathode side is consumed by the upstream regime and water accumulates at the downstream regime (channels 4–5 in Fig. 16) in the cell, there is a limited chemical reaction rate along channels 4–5. Additionally, the local water concentrations in regions A–D gradually decrease as the optimization process proceeds. At an optimal design, the local current density and liquid water are generally uniformly distributed over the entire membrane. The amount of water at the outlet in the optimal design is significantly less than that in the conventional design (step 1). The under-rib convection velocities are comparable to channel flow velocities; both increase with reduced channel heights. The strong convection flows enhance oxygen transport and water removal, leading to nearly uniform distributions of local current density in the membrane throughout the entire cell. Conversely, the final channel should be a diverging channel because strong under-rib convection occurring at the rib next to the outlet can result in considerable oxygen leakage and poor water removal for the final channel. The combined optimization has been proven effective in optimizing the flow-field design for a single serpentine PEMFC. The role of under-rib convection should be considered in cathode flow-field design.

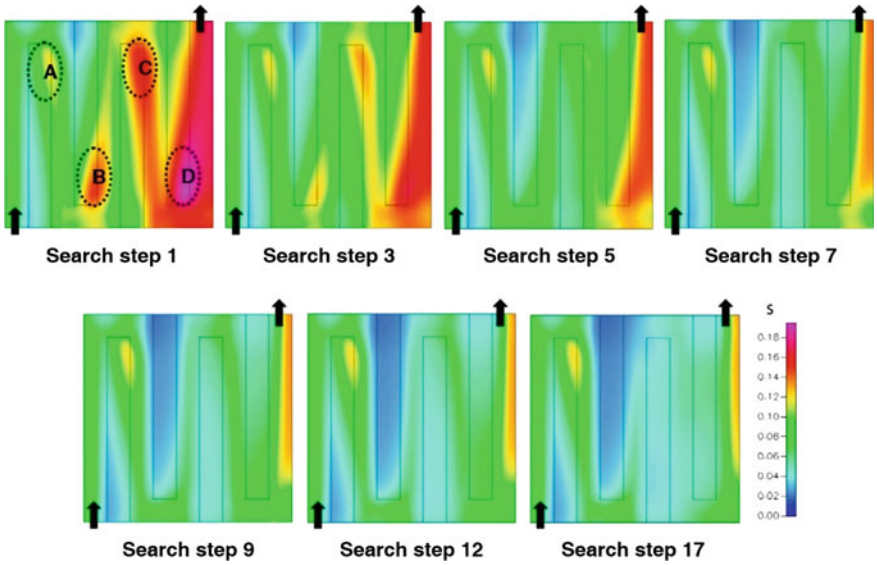


**Fig. 16** Liquid water distributions on the interface between the cathode gas diffusion layer and the catalyst layer at various search steps. *Numbers in the figure* denote each search step. *Source* Ref. [35]

## *4.4 Reduction in Pressure Drop*

The fuel flow channel has a GDL as a side-wall, and hence the GDL morphology is expected to influence the reactant gas transport from the channel to the catalyst surface and ultimately the cell performance. The design of this flow-field has a distinct influence on the oxygen transport from the GDL to the cathode catalyst layer. Although different designs have been examined, the choice of an optimal flow-field design still remains controversial. The parallel design avoids water accumulation in the corners of the flow-field and consequently avoids local starvation of the oxidant due to minimal pressure drop by equally distributing the flow rate into many straight parallel paths. Serpentine channel designs have been the most widely used because their increased channel length offers higher gas velocity in the channel with a moderate increase in parasitic loss by air pumping. This design ensures effective liquid water removal, which prevents channel clogging by condensate.

High power density requires high current density operation. Under these conditions, mass transport losses can be significant contributor to the overall loss mechanisms in the cell. When using air as the oxidant, the driving force for oxygen transport from channel to catalyst is low due to the low partial pressure. Oxygen needs to be transported from the feeding channel to the catalyst layer through a porous material. Besides, water that forms at the cathode catalyst can condense in the pores. A parameter study for was performed limiting current conditions;

this study emphasized the transport in the GDL between channels and did not require the complex description of the electrochemical kinetics [18]. The channel-rib geometry, channel-to-channel pressure difference and GDL characteristics were investigated in order to determine GDL design. To achieve a well-defined compression, the in-plane and the through-plane apparatuses were realized based on 30 mm thick stainless steel blocks. The distance was set by placing steel spacer plates between the blocks. A water column gauge with 1 Pa resolution was used to determine the pressure drop. To study the effects of cross convection in a serpentine channel, a 2D slice model of the GDL under the channel and rib was linked to a 3D model of a U-bend channel (simulating the serpentine flow-field). This 2D + 3D serpentine model was used to determine the local cross convection flow rates and the pressure distribution. To avoid excessive cross convection at the channel inlet where pressure gradients are high, a well thought out dimensioning of the channel-rib geometry and size of the additional GDL were imperative. The increased thickness under the rib also had the drawback of slightly increasing the electric resistance. In the light of the significant increase in the rib current and the relatively low Ohmic resistance of the GDL, the introduction of additional GDL material is expected to pay off in terms of overall performance.

The theory of the entrance region pressure drop was first introduced and validated in four-tube parallel channel geometry [13]. An experimental test section was designed to validate/modify the theoretical equations using water as the fluid. The equations derived for the developing laminar flow in circular ducts were used to describe the entrance region pressure drop within the tubes. The pressure drop in the tube entrance region was the summation of two components: a frictional pressure drop, which accounts for the greatest portion of the total pressure drop, and the minor pressure drop, caused by entrance region effects. For micro- and mini-channel applications, such as PEMFCs, laminar flow generally existed due to the relatively low flow rates and the small hydraulic diameters. A new technique was proposed to measure the instantaneous flow rate through individual channels in a parallel channel array. The experimental setup was specifically designed to allow calibration of the individual channel flow rates. The ability of this technique to accurately predict flow maldistribution in parallel channels was experimentally validated. The method was implemented in ex situ and in situ setups designed to study two-phase flow in gas diffusion channels of a PEMFC to develop effective water management strategies for PEMFCs. Based on the improvement of the local cross-flow conditions in a split serpentine flow-field [40], the overall flow rates in the three serpentine channels were within 5% of each other, showing that the flow distribution among the three serpentine channels was relatively uniform. The predicted pressure drop for the flow-field is only 2861 kPa, much less than the pressure drop of 25,665 kPa obtained with a single serpentine flow channel for the same air flow rate. Compared to the single serpentine, the flow rate through each of the three parallel paths was about 1/3. The path-length in each was also only one-third of the total serpentine path-length. Thus, the overall pressure drop, which was roughly equal to the pressure drop in one of the parallel paths, was 1/9 of the single serpentine.

To understand how a tapered flow channel and baffle plate affect the pressure drop, the dimensionless pressure drop between the gas fuel inlet and outlet across the channel was calculated [39]. Though, this design improved the fuel transport rate and enhanced the reaction at the catalyst layer, but the channel arrangement produced a larger pressure loss and required more pumping power for the delivery of the fuel. Therefore, with an appropriate gap and tapered ratios, the pressure drop as well as the pumping power can be considerably reduced. The convection-enhanced serpentine flow-field realized during this work showed superior performance compared to conventional serpentine flow-field due to its enhanced mass transport capability as a result of the enhanced under-rib convection associated with the increased pressure difference between adjacent flow channels [28]. Another striking feature of this new flow-field is that the pressure drop between the inlet and the outlet remains almost the same as that in the conventional design, because the channel dimensions, including width, depth, and total length, are the same for both flow-fields. The reduced gas flow rate will decrease the parasitic power in the fuel cell system, thus leading to higher system efficiency. It is worth mentioning that the convection-enhanced serpentine flow-field can also be readily extended to the formation of a flow-field consisting of multiple serpentines in parallel without losing the feature of enhanced under-rib convection and while resulting in a smaller pressure drop. The effects of the design parameters on the PEMFC performance have been examined using CFD calculation [26]. The numerical results based on a Taguchi L18 test matrix showed the output power and the pressure drop on the cathode and the anode sides for the current density of 1.2 A/cm$^2$, as shown in Fig. 17. It was evident that the power and the pressure drop results are affected by geometric design parameters. However, the appropriate pressure drop should be set because a high-pressure drop at the channel inevitably causes a high load on the Balance of Plants (BOP) system. Because more BOP resources result in lower net

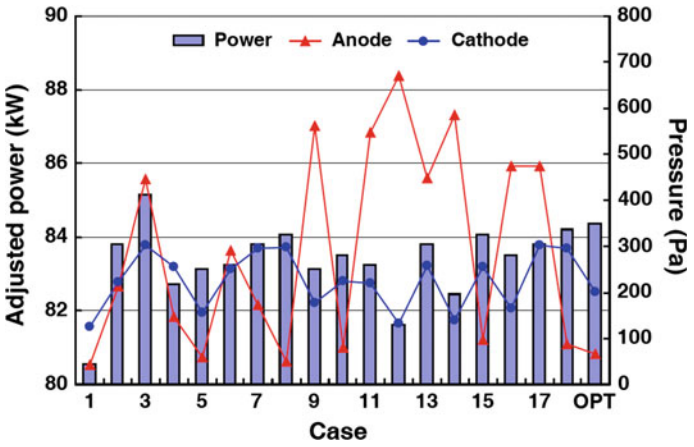


**Fig. 17** Power and pressure drop curve; at 1.2 A/cm$^2$ condition. *Source* Ref. [26]

power output from the system, it was necessary to design the bipolar plate with the maximum power and the minimum pressure drop. Based on the calculation of results, the power reaches its maximum in case 3, but the pressure drop is not at its minimum in this case. The set of optimum parameters obtained from the Taguchi method showed high power output with an appropriate pressure drop. There is an optimal combination of the design parameters through a trade-off between the performance and the pressure drop in the system design. The design parameters should be selected considering their effects on both the performance and the pressure drop in the channel in order to meet the goals of the PEMFC system.

## *4.5 Improvement in Output Power*

The cell output power increases with increasing active area, but not in proportional manner. This is attributed to the fact that long flow channels are commonly fabricated with cells of large active areas in order to provide high power which renders water removal difficult in maintaining a sufficient oxygen transfer rate at the cathode. In other words, the cell size effect is noticeable in PEMFC applications. However, to the best of our knowledge, at present the size effect has not yet been satisfactorily analyzed. Performance curves of PEMFCs were investigated for parallel flow-fields with various active areas [34]. The cathode and anode flow channels formed a rectangular shape with $1 \times 1$ mm$^2$ ribs. The active area of cell 1 was $11 \times 11$ mm$^2$ with 6 channels and 5 ribs; the active area of cell 2 was $21 \times 21$ mm$^2$ with 11 channels and 10 ribs; the active area of cell 3 was $31 \times 31$ mm$^2$ with 16 channels and 15 ribs; and the active of cell 4 was $41 \times 41$ mm$^2$ with 21 channels and 20 ribs. Moreover, because the reactant inlet flow rates significantly affect the cell performance, for convenience of comparison, specified inlet flow rates were fed to the unit active area for all cells in the present work with 0.4 cm$^3$/min humidified hydrogen to 1 mm$^2$ active area on the anode side, and 1.2 cm$^3$/min humidified air to 1 mm$^2$ active area on the cathode side. For operating voltages >0.7 V, the polarization curves and power density curves for four active areas almost coincided, indicating negligible cell size effects. However, at operating voltages <0.7 V, the size effect was profound. The average current density and output power density all decreased with an increase in the active area. As the active area was increased from $11 \times 11$ mm$^2$ to $41 \times 41$ mm$^2$ (by 13.9 times), the average current density decreased by 10.6% at 0.4 V and 11.6% at 0.3 V. Three different channel heights and widths were compared with the base flow-field design of the serpentine channel that was 1 mm wide and 0.34 mm high, each through a detailed numerical study of the distribution of temperature, pressure, water content, and local current density [41]. The output power density is lowered due to the decreased cell voltage and larger volume of PEMFC stack with the channel height. The cell voltage was decreased with the increase of channel width, and its extent of the reduction was larger than that with the increased channel height.

The optimal cathode flow-field design of a single serpentine proton exchange membrane fuel cell was obtained by adopting a combined optimization procedure including a simplified conjugate-gradient method and a completely three-dimensional, two-phase, non-isothermal fuel cell model, to look for optimal flow-field design for a single serpentine fuel cell $9 \times 9$ mm$^2$ in size with five channels [30]. The initial guess assumed all channel heights and widths of 1 mm, identical to the basic design with straight channels. The cell output power density $P_{\text{cell}}$ was maximized and subjected to an optimal set of channel heights, $H_1$–$H_5$, and channel widths, $W_2$–$W_5$. The basic case with all channel heights and widths set at 1 mm yielded a $P_{\text{cell}} = 7260$ W/m$^2$. The optimal design displays a tapered characteristic for channels 1, 3, and 4, and a diverging characteristic in height for channels 2 and 5, producing a $P_{\text{cell}} = 8894$ W/m$^2$, about a 22.5% increment. The reduced channel heights of channels 2–4 significantly increased the under-rib convection and widths for effectively removing liquid water and oxygen transport in the gas diffusion layer. The final diverging channel minimized the leakage of fuel to outlet via under-rib convection from channels 4 to 5. The use of a straight, final channel of 0.1 mm height led to a 7.37% power loss, whereas designing all channel widths to be 1 mm with optimal channel heights obtained the above yields with only a 1.68% loss in current density.

The serpentine flow channel layout is not the ideal flow-field configuration, and this layout has a number of problems. It typically results in a relatively long reactant flow path, hence a substantial pressure drop, resulting in significant parasitic power loss associated with the cathode air supply (as much as 35% or more of the stack output power). A novel serpentine-baffle flow-field design was proposed to improve the cell performance compared to that of a conventional serpentine flow-field using a three-dimensional numerical model [29]. The flow-field design influenced not only the cell performance but also the pressure drop in the fuel cell. Larger pressure drops in the fuel cell meant that more power was needed to pump the reactants. Thus, the pressure drop is a significant issue to be considered in choosing the flow-field designs in addition to the $I$–$V_{\text{cell}}$ curve. The pressure drops for baffled designs were higher than those for the conventional design, and then the cathode pressure drop loss, $W_P$, was calculated. Although the pressure drops for the baffled designs are larger than those for the conventional design, the pressure drop losses, $W_P$, were far lower than the cell output power, $P_{\text{cell}}$, for the miniature fuel cells analyzed.

A concise mathematical model was developed for quick numerical simulation to allow performance prediction and analysis of DMFC [31]. Two-phase flow at the anode and pressure-driven convection were both included in the proposed model and thereby enabled accurate and realistic performance prediction and analysis. To investigate the two-phase mass transport effect on cell performance, the $I$–$V$ curve for 1 M input methanol at 40 °C was simulated. The liquid saturation $S$ was assumed to be unity and thereby represented the transport of only liquid phase at the anode. The limiting current density 147.0 mA/cm$^2$ was much smaller than that assigned for two-phase mass transport, viz., 200.6 mA/cm$^2$ by under-rib mass transport effect. The results thus revealed that methanol transport in the gas phase is important for sufficient fuel supply to the reaction sites. Moreover, the cell voltage

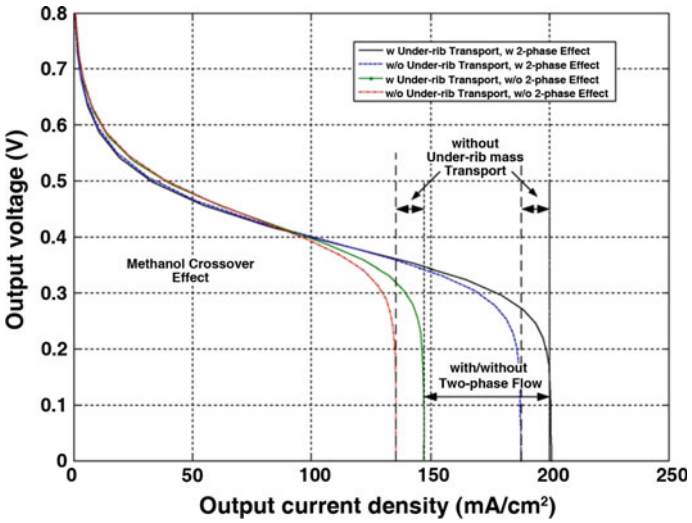


**Fig. 18** Influence of two-phase flow phenomenon on DMFC performance, with and without under-rib mass transport consideration effects; 1 M input methanol solution with 2 ml/min flow rate at 40 °C operating temperature. *Source* Ref. [31]

reduction induced by methanol crossover was noted at a low current density where the liquid phase transport situation gave a higher cell output voltage compared with that for two-phase transport. Consequently, the limiting current density had a relatively small value of 135.5 mA/cm$^2$. That is reasonably close to the modeling result of 138.4 mA/cm$^2$. The difference between including or not including the under-rib mass transport effect implied that the facilitated methanol transport towards the catalyst layer was influenced by under-rib mass transport. The significance of under-rib mass transport on performance was, however, less than that caused by the two-phase effect. Performance data with the under-rib mass transport effect subtracted from the two-phase mass transport are presented in Fig. 18.

As shown in Fig. 19, numerical simulations were performed to compare the four configurations: configuration I in which CASFFs were used both at the anode and the cathode; configuration II in which a SFFSB and a CASFF were used at the anode and the cathode, respectively, configuration III in which SFFSBs were used at both the anode and the cathode, and configuration IV in which a CASFF and a SFFSB were used at the anode and the cathode, respectively. To verify the maximization of power density among the performance-related parameters, the polarization and power density curves for different flow-field configurations I–IV obtained by numerical simulation are compared, and the results are shown in Fig. 20a. The results reveal that the power densities of configurations III and IV are higher in comparison with the flow-field configurations I and II. Maximum power densities of the four flow-field configurations I–IV are 0.5199, 0.5278, 0.6122 and 0.6175 W/cm$^2$, respectively. The adoption of SFFSB at the cathode bipolar plate

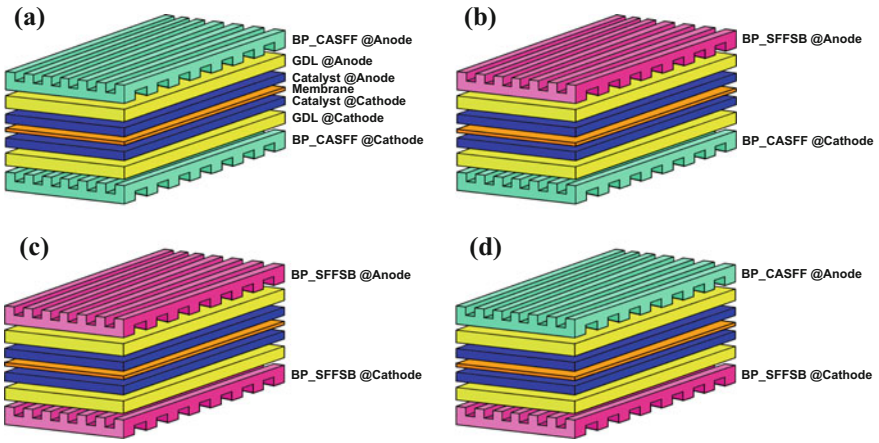


**Fig. 19** Four flow-field configurations of CASFF and SFFSB applied on the anode and cathode bipolar plates: **a** configuration I in which CASFFs were used at both the anode and the cathode; **b** configuration II in which a SFFSB and a CASFF were used at the anode and the cathode, respectively; **c** configuration III in which SFFSBs were used at both the anode and the cathode; **d** configuration IV in which a CASFF and a SFFSB were used at the anode and the cathode, respectively

increases the output power density because the under-rib convection enables a more effective utilization of the electrocatalysts by increasing the mass transport rates of the reactants from the flow channel to the inner catalyst layer and by significantly reducing the water flooding at the cathode.

Figure 20b shows that the experimental results for the polarization and power density curves obtained with the CASFF and SFFSB have the same trend as the simulation results. The PEMFC performances with 5 passes and 4 turns on an active area of 25 $cm^2$ were experimentally evaluated for a new flow-field design, which stimulates under-rib convection by adding sub-channels and by-pass areas to the CASFF. Although the activation loss region and the ohmic resistance loss region exhibit almost the same characteristics, a small performance variation occurs in the mass transport loss region. This variation is caused by worsening water management conditions for moving toward the higher current density zone because the height of the channel is shorter due to the flow-field patterns, even though the cell went through an adequate activation process. The fuel cell performance is affected by the internal behavior, and it is especially sensitive to the behavior of the liquid water in the electrochemical reaction. The behavior of the liquid water inside the flow-field increases the water content of the MEA at the beginning of fuel cell operation, and it usually moves from the anode to the cathode. However, back diffusion sometimes occurs due to the liquid water mass fraction and the pressure drop of the cathode. Furthermore, the liquid water cools the heat caused by the electrochemical reaction. The behavior of the liquid water becomes one of the determining factors for cell performance. By adding the sub-channels and the

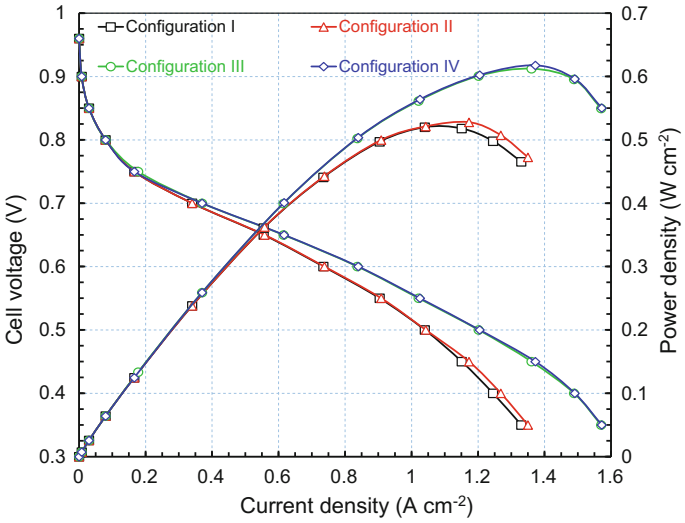


(a) Comparisons of numerical results

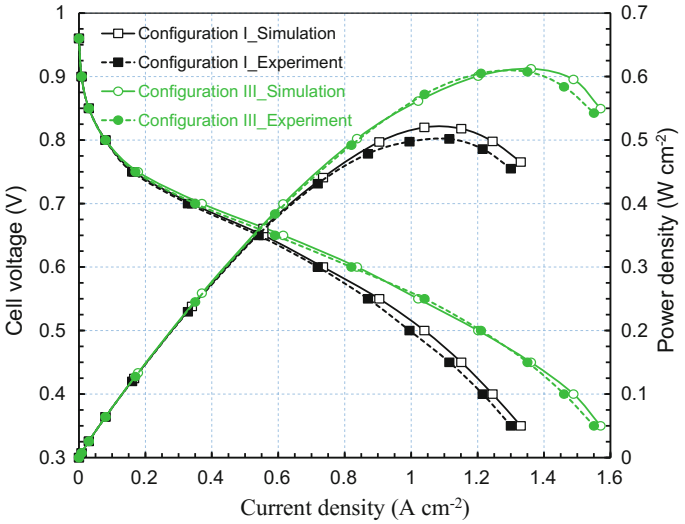


(b) Comparison of experimental and numerical results

**Fig. 20** Comparisons of the polarization and power density curves: **a** between the four flow-field configurations I–IV obtained by numerical simulation; between the experimental and simulation results of the flow-field configurations I and III

bypasses to the CASFF, the SFFSB improves the flow consistency of the inner reaction gas and the liquid water behavior, and it enhances the current density in both ohmic resistance loss region and the mass transport loss region [165].

## 5 Summary

In this article, the research and development in PEMFCs, ranging from their components (PEM, electrodes and catalysts, GDL, MEA and bipolar plates) and cells (single cell and multi-cell stack), as well as the experimental and modeling approaches for the optimization of flow-field, followed by the new flow-field optimization using under-rib convection have been discussed. Although the performance of PEMFCs is primarily determined by the intrinsic electrochemical efficiency of the MEA, the flow plate is one of the key components of a PEMFC, serving as both the current collector and the reactant distributor. The uniform distribution of reactants over the entire surface of the fuel cell catalyst layer also depends on the design of the porous diffusion layer, including pore size and the thickness of the porous diffusion layer. Recently, the effects of under-rib convection on mass and heat transport, liquid water removal as well as pressure drop have related to PEMFCs been actively investigated.

The under-rib convection enables more effective utilization of electrocatalysts by increasing reactant concentration and promotes the uniformity of temperature and current density distributions. If facilitates liquid water discharge, reduces the pressure drop, and improves output power. Although much progress has been made with respect to flow-field optimization, discussions of optimal flow-field designs still remained controversial. Development of new flow-fields via the promotional role of under-rib convection has been suggested; however, some challenges remain regarding the new flow plates issues such as the volume, weight, and cost of PEMFC stacks.

First, the electrochemical and physical properties, which are verified not by invalidated measurements but by standard measurements in an operating fuel cell, are essential to bridging the gap between modeling and experiments. The validation of experimental results by modeling provides qualitative comparison, and hence numerical models have been quantitatively verified. Recently, segment-wise pressure distribution data have revealed how to optimize the clamping pressure using the developed setup for a given GDL for uniform reactant distributions and pressure drop behaviors [166]. Simulation results have been compared quantitatively to the bubble velocities and geometric dimensions observed in the experimental data of both coated and uncoated channels [167].

Second, there is a need to apply the developed flow plate to a practical PEMFC stack and validate the effects of under-rib convection on water and heat management, pressure drops, and output power. Under-rib convection is a complex phenomenon in which the mass transport of reactants in flow plates as well as GDL and catalysts influence liquid water, pressure, temperature and current density.

Therefore, the advanced flow plates, which were developed to promote under-rib convection, should be confirmed as playing a promotional role in the flow plates at the same time in order to meet the goal of the PEMFC system. For example, this situation can be seen in comparing the output power and the pressure drop loaded on the BOP [26].

This review has shown that the new flow-field optimization technique by under-rib convection has great potential for improving cell performances inside operating PEMFCs. The flow-field that activates the internal mass transfer mechanism of PEMFCs is able to improve its power density from a mechanical engineering perspective. In other words, this mechanical method can improve the performance of the fuel cells without changing the electrochemical materials. An approach combining fundamental study and engineering development of under-rib convection would help us take the necessary steps to advance the performance and commercialize PEMFCs.

## References

1. Barbir F (2005) PEM fuel cells: theory and practice. Elsevier, London
2. O'Hayre RP, Cha SW, Colelle W, Prinz FB (2006) Fuel cell fundamentals. Wiley, New York
3. Bose S, Kuila T et al (2011) Polymer membranes for high temperature proton exchange membrane fuel cell: recent advances and challenges. Prog Polym Sci 36(6):813–843
4. Gasteiger HA, Panels JE, Yan SG (2004) Dependence of PEM fuel cell performance on catalyst loading. J Power Sources 127(1):162–171
5. Dohle H, Jung R, Kimiaie N, Mergel J, Müller M (2003) Interaction between the diffusion layer and the flow field of polymer electrolyte fuel cells: experiments and simulation studies. J Power Sources 124(2):371–384
6. Wilkinson DP, Zhang J, Hui R, Fergus J, Li X (2010) Proton exchange membrane fuel cells: materials properties and performance. In: Lee S (ed) Green chemistry and chemistry engineering. CRC Press, New York
7. Nguyen TV (1996) A gas distributor design for proton-exchange-membrane fuel cells. J Electrochem Soc 143(5):103–105
8. Li X, Sabir I (2005) Review of bipolar plates in PEM fuel cells: flow-field designs. Int J Hydrogen Energy 30(4):359–371
9. Zhang L, Bi HT, Wilkinson DP, Stumper J, Wang H (2008) Gas–liquid two-phase flow patterns in parallel channels for fuel cells. J Power Sources 183(2):643–650
10. Pharoah JG (2005) On the permeability of gas diffusion media used in PEM fuel cells. J Power Sources 144(1):77–82
11. Inoue G, Matsukuma Y, Minemoto M (2006) Effect of gas channel depth on current density distribution of polymer electrolyte fuel cell by numerical analysis including gas flow through gas diffusion layer. J Power Sources 157(1):136–152
12. Dutta S, Shimpalee S, Van Zee JW (2001) Numerical prediction of mass-exchange between cathode and anode channels in a PEM fuel cell. Int J Heat Mass Transfer 44(11):2029–2042
13. Kandlikar SG, Lu Z, Domigan WE, White AD, Benedict MW (2009) Measurement of flow maldistribution in parallel channels and its application to ex-situ and in-situ experiments in PEMFC water management studies. Int J Heat Mass Transfer 52(7):1741–1752

14. Williams MV, Kunz HR, Fenton JM (2004) Influence of convection through gas-diffusion layers on limiting current in PEMFCs using a serpentine flow field. J Electrochem Soc 151(10):1617–1627
15. Oosthuizen PH, Sun L, McAuley KB (2005) The effect of channel-to-channel gas crossover on the pressure and temperature distribution in PEM fuel cell flow plates. Appl Therm Eng 25(7):1083–1096
16. Sun L, Oosthuizen PH, McAuley KB (2006) A numerical study of channel-to-channel flow cross-over through the gas diffusion layer in a PEM-fuel-cell flow system using a serpentine channel with a trapezoidal cross-sectional shape. Int J Therm Sci 45:1021–1026
17. Prasad KBS, Jayanti S (2008) Effect of channel-to-channel cross-flow on local flooding in serpentine flow-fields. J Power Sources 180(1):227–231
18. Tehlar D, Flückiger R, Wokaun A, Büchi FN (2010) Investigation of channel-to-channel cross convection in serpentine flow fields. Fuel Cells 10(6):1040–1049
19. Sun W, Peppley BA, Karan K (2005) Modeling the influence of GDL and flow-field plate parameters on the reaction distribution in the PEMFC cathode catalyst layer. J Power Sources 144(1):42–53
20. Wang Y, Wang CY (2005) Simulation of flow and transport phenomena in a polymer electrolyte fuel cell under low-humidity operation. J Power Sources 147(1):148–161
21. Kanezaki T, Li X, Baschuk JJ (2006) Cross-leakage flow between adjacent flow channels in PEM fuel cells. J Power Sources 162(1):415–425
22. Feser JP, Prasad AK, Advani SG (2006) On the relative influence of convection in serpentine flow fields of PEM fuel cells. J Power Sources 161(1):404–412
23. Ye Q, Zhao TS, Xu C (2006) The role of under-rib convection in mass transport of methanol through the serpentine flow field and its neighboring porous layer in a DMFC. Electrochim Acta 51(25):5420–5429
24. Park J, Li X (2007) An experimental and numerical investigation on the cross flow through gas diffusion layer in a PEM fuel cell with a serpentine flow channel. J Power Sources 163(2):853–863
25. Li X, Sabir I, Park J (2007) Review of bipolar plates in PEM fuel cells: flow-field designs. J Power Sources 30(4):359–371
26. Lee S, Jeong H, Ahn B, Lim T, Son Y (2008) Parametric study of the channel design at the bipolar plate in PEMFC performances. Int J Hydrogen Energy 30(20):5691–5696
27. Xu C, He YI, Zhao TS, Chen R, Ye Q (2006) Analysis of mass transport of methanol at the anode of a direct methanol fuel cell. J Electrochem Soc 153(7):1358–1364
28. Xu C, Zhao TS (2007) A new flow field design for polymer electrolyte-based fuel cells. Electrochem Commun 9(3):497–503
29. Wang XD, Duan YY, Yan WM (2007) Novel serpentine-baffle flow field design for proton exchange membrane fuel cells. J Power Sources 173(1):210–221
30. Wang WD, Huang YX, Cheng CH, Jang JY, Lee DJ, Yan WM, Su S (2009) Flow field optimization for proton exchange membrane fuel cells with varying channel heights and widths. Electrochim Acta 54(23):5522–5530
31. Yang Y, Liang YC (2009) Modelling and analysis of a direct methanol fuel cell with under-rib mass transport and two-phase flow at the anode. J Power Sources 194(2):712–729
32. Nam JH, Lee KJ, Sohn S, Kim CJ (2009) Multi-pass serpentine flow-fields to enhance under-rib convection in polymer electrolyte membrane fuel cells: design and geometrical characterization. J Power Sources 188(1):14–23
33. Wang XD, Duan YY, Yan WM, Lee DJ, Su A, Chi PH (2009) Channel aspect ratio effect for serpentine proton exchange membrane fuel cell: role of sub-rib convection. J Power Sources 193(2):684–690
34. Wang XD, Zhang XX, Yan WM, Lee DJ, Su A (2009) Determination of the optimal active area for proton exchange membrane fuel cells with parallel, interdigitated or serpentine designs. Int J Hydrogen Energy 34(9):3823–3832

35. Wang XD, Huang YX, Cheng CH, Jang JY, Lee DJ, Yan WM, Su A (2010) An inverse geometry design problem for optimization of single serpentine flow field of PEM fuel cell. Int J Hydrogen Energy 35(9):4247–4257
36. Zhang Y, Zhang P, Zhenyu Y, He H, Zhao Y, Liu X (2011) A tapered serpentine flow field for the anode of micro direct methanol fuel cells. J Power Sources 196(6):3255–3259
37. Baek SM, Koh SG, Kim KN, Kang JH, Nam JH, Kim CH (2011) A numerical study on the performance of polymer electrolyte membrane fuel cells due to the variation in gas diffusion layer permeabilities. J Mech Sci Technol 25(2):457–467
38. Wang XD, Xu JL, Yan WM, Lee DJ, Su A (2011) Transient response of PEM fuel cells with parallel and interdigitated flow field designs. Int J Heat Mass Transfer 54(11):2375–2386
39. Perng SW, Wu HW (2011) Non-isothermal transport phenomenon and cell performance of a cathodic PEM fuel cell with a baffle plate in a tapered channel. Appl Energy 88(1):52–67
40. Suresh PV, Jayanti S, Deshpande AP, Haridoss P (2011) An improved serpentine flow field with enhanced cross-flow for fuel cell applications. Int J Hydrogen Energy 36(10):6067–6072
41. Choi KS, Kim HM, Moon SM (2011) Numerical studies on the geometrical characterization of serpentine flow-field for efficient PEMFC. Int J Hydrogen Energy 36(2):1613–1627
42. Choi KS, Kim HM, Moon SM (2011) An experimental study on the enhancement of the water balance, electrochemical reaction and power density of the polymer electrolyte fuel cell by under-rib convection. Electrochem Commun 13(12):1387–1390
43. Costamagna P, Srinvasan S (2001) Quantum jumps in the PEMFC science and technology from the 1960s to the year 2000: Part I. Fundamental scientific aspects. J Power Sources 102(1):242–252
44. Costamagna P, Srinvasan S (2001) Quantum jumps in the PEMFC science and technology from the 1960s to the year 2000: Part II. Engineering, technology development and application aspects. J Power Sources 102(1):253–269
45. Gamburzev S, Appleby AJ (2002) Recent progress in performance improvement of the proton exchange membrane fuel cell (PEMFC). J Power Sources 107(1):5–12
46. Mehta V, Cooper JS (2003) Review and analysis of PEM fuel cell design and manufacturing. J Power Sources 114(1):32–53
47. Haraldsson K, Wipke K (2004) Evaluating PEM fuel cell system models. J Power Sources 126(1):88–97
48. Yao KZ, Karan K, McAuley KB, Oosthuizen P, Peppley B, Xie T (2004) Review of mathematical models for hydrogen and direct methanol polymer electrolyte membrane fuel cells. Fuel Cells 4(1):3–29
49. Brykoğlu A (2005) Review of proton exchange membrane fuel cell models. Int J Hydrogen Energy 30(11):1181–1212
50. Cheddie D, Munroe N (2005) Review and comparison of approaches to proton exchange membrane fuel cell modeling. J Power Sources 147(1):72–84
51. Faghri A, Guo Z (2005) Challenges and opportunities of thermal management issues related to fuel cell technology and modeling. Int J Heat Mass Transfer 48(19):3891–3920
52. Hermann A, Chaudhuri T, Spagnol P (2005) Bipolar plates for PEM fuel cells: a review. Int J Hydrogen Energy 30(12):1297–1302
53. Smitha B, Sridhar S, Khan AA (2005) Solid polymer electrolyte membranes for fuel cell applications: a review. J Membr Sci 259(1):10–26
54. Pettersson J, Ramsey B, Harrison D (2006) A review of the latest developments in electrodes for unitised regenerative polymer electrolyte fuel cells. J Power Sources 157(1):28–34
55. Tawfik H, Hung Y, Mahajan D (2007) Metal bipolar plates for PEM fuel cell: a review. J Power Sources 163(2):755–767
56. Neburchilov V, Martin J, Wang H, Zhang J (2007) A review of polymer electrolyte membranes for direct methanol fuel cells. J Power Sources 169(2):221–238
57. Djilali N (2007) Energy computational modelling of polymer electrolyte membrane (PEM) fuel cells: challenges and opportunities. Energy 32(4):269–280

58. De Bruijn FA, Dam VAT, Janssen GJM (2008) Review: durability and degradation issues of PEM fuel cell components. Fuel Cells 8(1):3–22
59. Siegel C (2008) Review of computational heat and mass transfer modeling in polymer-electrolyte-membrane (PEM) fuel cells. Energy 33(9):1331–1352
60. Peighambardoust SJ, Rowshanzamir S, Amjadi M (2010) Review of the proton exchange membranes for fuel cell applications. Int J Hydrogen Energy 35(17):9349–9384
61. Antunes RA, Oliveira MCL, Ett G, Ett V (2010) Corrosion of metal bipolar plates for PEM fuel cells: a review. Int J Hydrogen Energy 35(8):3632–3647
62. Krivobokov IM, Gribov EN, Qkunev AG (2011) Proton conducting hydrocarbon membranes: Performance evaluation for room temperature direct methanol fuel cells. Electrochim Acta 56(5):2420–2427
63. Tsushima S, Hirai S (2011) In situ diagnostics for water transport in proton exchange membrane fuel cells. Prog Energy Combust Sci 37(2):204–220
64. Sengupta R, Bhattacharya M, Bandyopadhyay S, Bhowmick A (2011) A review on the mechanical and electrical properties of graphite and modified graphite reinforced polymer composites. Prog Polym Sci 36(5):638–670
65. Chang JH, Park JH, Park GG, Kim CS, Park OO (2003) Proton-conducting composite membranes derived from sulfonated hydrocarbon and inorganic materials. J Power Sources 127(1):18–25
66. Wakizoe M, Velev OA, Srinivasan S (1995) Analysis of proton-exchange membrane fuel-cell performance with alternate membranes. Electrochim Acta 40(3):335–344
67. Liu W, Zuckerboard D (2005) In situ detection of hydrogen peroxide in PEM fuel cells. J Electrochem Soc 152(6):1165–1170
68. Scherer GG, Bunsen-Ges B (1990) Polymer membranes for fuel cells. Phys Chem 94(9): 1008–1014
69. Qiao J, Saito M, Hayamizu K, Tokadaz T (2006) Degradation of perfluorinated ionomer membranes for PEM fuel cells during processing with $H_2O_2$. J Electrochem Soc 153(6):967–974
70. Teranishi K, Kawata K, Tsushima S, Hirai S (2006) Degradation mechanism of PEMFC under open circuit operation. Electrochem Solid-State Lett 9(10):475–477
71. Trogadas P, Parrondo J, Ramani V (2008) Degradation mitigation in polymer electrolyte membranes using cerium oxide as a regenerative free-radical scavenger. Electrochem Solid-State Lett 11(7):113–116
72. Healy J, Hayden C et al (2005) Aspects of the chemical degradation of PFSA ionomers used in PEM fuel cells. Fuel Cells 5(2):302–308
73. Liu W, Ruth K, Rusch G (2001) Membrane durability in PEM fuel cells. J New Mat Electr sys 4(4):227–232
74. Kyu T, Hashiyama M, Eisenberg A (1983) Dynamic mechanical studies of partially ionized and neutralized Nafion polymers. Can J Chem 61(4):680–687
75. Mukerjee S, Srinivasan S (1993) Enhanced electrocatalysis of oxygen reduction on platinum alloys in proton exchange membrane fuel cells. J Electroanal Chem 357(1):201–224
76. Swette LL, LaConti AB, McCatty SA (1994) Proton-exchange membrane regenerative fuel cells. J Power Sources 47(3):343–351
77. Borup R, Meyers J et al (2007) Scientific aspects of polymer electrolyte fuel cell durability and degradation. Chem Rev 107(10):3904–3951
78. Stevens DA, Dahn JR (2005) Thermal degradation of the support in carbon-supported platinum electrocatalysts for PEM fuel cells. Carbon 43(1):179–188
79. Cai M, Ruthkosky MS et al (2006) Investigation of thermal and electrochemical degradation of fuel cell catalysts. J Power Sources 160(2):977–986
80. Schulze M, Wagner N, Kaz T, Friedrich KA (2007) Combined electrochemical and surface analysis investigation of degradation processes in polymer electrolyte membrane fuel cells. Electrochim Acta 52(6):2328–2336
81. St-Pierre J, Wilkins DP, Knights S, Bos ML (2000) Relationships between water management, contamination and lifetime degradation in PEFC. J New Mat Electr Syst 3:99–106

82. Jordan LR, Shukla AK, Behrsing T, Avery NR, Muddle BC, Forsyth M (2000) Diffusion layer parameters influencing optimal fuel cell performance. J Power Sources 86(1):250–254
83. Pasaogullari U, Wang CY (2004) Two-phase transport and the role of micro-porous layer in polymer electrolyte fuel cells. Electrochim Acta 49(25):4359–4369
84. Pasaogullari U, Wang CY, Chen KS (2005) Two-phase transport in polymer electrolyte fuel cells with bilayer cathode gas diffusion media. J Electrochem Soc 152(8):1574–1582
85. Weber AZ, Darling RM, Newman J (2004) Modeling two-phase behavior in PEFCs. J Electrochem Soc 151(10):1715–1727
86. Weber AZ, Newman J (2005) Effects of microporous layers in polymer electrolyte fuel cells. J Electrochem Soc 152(4):677–688
87. Lee C, Mérida W (2007) Gas diffusion layer durability under steady-state and freezing conditions. J Power Sources 164(1):141–153
88. Raistrick ID (1990) Impedance studies of porous electrodes. Electrochim Acta 35(10): 1579–1586
89. Dhar HP (1997) Study of combined electroreflectance and double layer effects at lead electrodes. Surf Sci 66(2):449–462
90. Gottesfeld S, Zawodzinski TA (1997) In polymer electrolyte fuel cells. Wiley, Weinheim
91. Tsuchiya H, Kobayashi O (2004) Mass production cost of PEM fuel cell by learning curve. Int J Hydrogen Energy 29(10):985–990
92. Cooper JS (2004) Design analysis of PEMFC bipolar plates considering stack manufacturing and environment impact. J Power Sources 129(2):152–169
93. Müller A, Kauranen P, Von Ganski A, Hell B (2006) Injection moulding of graphite composite bipolar plates. J Power Sources 154(2):467–471
94. Maheshwari PH, Mathur RB, Dhami TL (2007) Fabrication of high strength and a low weight composite bipolar plate for fuel cell applications. J Power Sources 173(1):394–403
95. Pozio A, Silva RF, Fancesco DM, Giorgi L (2003) Nafion degradation in PEFCs from end plate iron contamination. Electrochim Acta 48(11):1543–1549
96. Wind J, Späh R, Kaiser W, Böhm G (2002) Metallic bipolar plates for PEM fuel cells. J Power Sources 105(2):256–260
97. Shimpalee S, Ohashi M et al (2009) Experimental and numerical studies of portable PEMFC stack. Electrochim Acta 54(10):2899–2911
98. Malkow T, Thalau O et al (2010) PEFC power stack performance testing procedure, test module PEFC ST 5-6. Publications Office of the European Union, Luxembourg
99. Tripathi BP, Shahi VK (2011) Organic–inorganic nanocomposite polymer electrolyte membranes for fuel cell applications. Prog Polym Sci 36(7):945–979
100. Rhee CH, Kim HK, Chang H, Lee JS (2005) Nafion/sulfonated montmorillonite composite: a new concept electrolyte membrane for direct methanol fuel cells. Chem Mater 17(7): 1691–1697
101. Watanabe M, Satoh Y, Shimura C (1993) Management of the water vontent in polymer electrolyte membranes with porous fiber wicks. J Electrochem Soc 140(11):3190–3193
102. Miachon S, Aldebert P (1995) Internal hydration H2/O2 100 $cm^2$ polymer electrolyte membrane fuel cell. J Power Sources 56(1):31–36
103. Choi KS, Kim HM, Yoon YC, Forrest ME, Erickson PA (2008) Effects of ambient temperature and relative humidity on the performance of Nexa fuel cell. Energ Convers Manage 49(12):3505–3511
104. Kandlikar SG, Lu Z (2009) Thermal management issues in a PEMFC stack—a brief review of current status. Appl Therm Eng 29(7):1276–1280
105. Heinzel A, Barragán VM (1999) A review of the state-of-the-art of the methanol crossover in direct methanol fuel cells. J Power Sources 84(1):70–74
106. Wasmus S, Küver A (1999) Methanol oxidation and direct methanol fuel cells: a selective review. J Electroanal Chem 461(1):14–31
107. Liu L, Pu C, Viswanathan R, Fan Q, Liu L, Smotkin ES (1998) Carbon supported and unsupported Pt–Ru anodes for liquid feed direct methanol fuel cells. Electrochim Acta 43(24):3657–3663

108. Page T, Johnson R, Hormes J, Nording S, Rambabu B (2000) A study of methanol electro-oxidation reactions in carbon membrane electrodes and structural properties of Pt alloy electro-catalysts by EXAFS. J Electroanal Chem 485(1):34–41
109. Ren X, Springer TE, Gottesfeld S (2000) Water and methanol uptakes in Nafion membranes and membrane effects on direct methanol cell performance. J Electrochem Soc 147(1):92–98
110. Baschuk JJ, Li X (2001) Carbon monoxide poisoning of proton exchange membrane fuel cells. Int J Energy Res 25(8):695–713
111. Gang X, Qingfeng L, Hjuler HA, Bjerrum NJ (1995) Hydrogen oxidation on gas diffusion electrodes for phosphoric acid fuel cells in the presence of carbon monoxide and oxygen. J Electrochem Soc 142(9):2890–2893
112. Doyle M, Rajendran G (2003) Handbook of fuel cells. Wiley, England
113. Wilkinson DP, Voss HH, Prater K (1994) Water management and stack design for solid polymer fuel cells. J Power Sources 49(1):117–127
114. Mosdale R, Srinivasan S (1995) Analysis of performance and of water and thermal management in proton exchange membrane fuel cells. Electrochim Acta 40(4):413–421
115. Squadrito G, Barbera O, Giacoppo G, Urbani F, Passalacqua E (2008) Polymer electrolyte fuel cell stack research and development. Int J Hydrogen Energy 33(7):1941–1946
116. Zhai Y, Zhang H, Zhang Y, Xing D (2007) A novel $H_3PO_4$/Nafion–PBI composite membrane for enhanced durability of high temperature PEM fuel cells. J Power Sources 169(2):259–264
117. Zhai Y, Zhang H, Liu G, Hu J, Yi B (2007) Degradation study on MEA in $H_3PO_4$/PBI High-temperature PEMFC life test. J Electrochem Soc 154(1):72–76
118. Cleghorn SJC, Mayfield DK et al (2006) A polymer electrolyte fuel cell life test: 3 years of continuous operation. J Power Sources 158(1):446–454
119. Choi KS, Jang SH, Shin GS, Kim HM, Yoon HC, Forrest ME, Erickson PA (2010) Effects of stack array orientation on fuel cell efficiency for auxiliary power unit applications. Int J Automot Techn 11(3):429–434
120. Ghosh PC, Wuster T, Dohle H, Kimiaie N, Mergel J, Stolten D (2006) In situ approach for current distribution measurement in fuel cells. J Power Sources 154(1):184–191
121. Stumper J, Campbell SA, Wilkinson DP, Johnson MC, Davis M (1998) In-situ methods for the determination of current distributions in PEM fuel cells. Electrochim Acta 43(24):3773–3783
122. Hakenjos A, Muenter H, Wittstadt U, Hebling C (2004) A PEM fuel cell for combined measurement of current and temperature distribution, and flow field flooding. J Power Sources 131(1):213–216
123. Park K, Kim HK, Choi KS (2013) Numerical and experimental verification of the polymer electrolyte fuel cell performances enhanced by under-rib convection. Fuel Cells 13(5):927–934
124. Hogarth WHJ, Steiner J, Benziger JB, Hakenjos A (2007) Spatially-resolved current and impedance analysis of a stirred tank reactor and serpentine fuel cell flow-field at low relative humidity. J Power Sources 164(2):464–471
125. Freunberger SA, Reum M, Wokaun A, Büchi FN (2006) Expanding current distribution measurement in PEFCs to sub-millimeter resolution. Electrochem Commun 8(9):1435–1438
126. Higier A, Liu H (2010) Optimization of PEM fuel cell flow field via local current density measurement. Int J Hydrogen Energy 35(5):2144–2150
127. Alaefour I, Karimi G, Jiao K, Li X (2011) Measurement of current distribution in a proton exchange membrane fuel cell with various flow arrangements—a parametric study. Appl Energy 93:80–89
128. Peng L, Mai J, Hu P, Lai X, Lin Z (2011) Optimum design of the slotted-interdigitated channels flow field for proton exchange membrane fuel cells with consideration of the gas diffusion layer intrusion. Renew Energ 36(5):1413–1420
129. Takada K, Ishigami Y et al (2011) Simultaneous visualization of oxygen distribution and water blockages in an operating triple-serpentine polymer electrolyte fuel cell. J Power Sources 196(5):2635–2639

130. Ishigami Y, Takada K et al (2011) Corrosion of carbon supports at cathode during hydrogen/air replacement at anode studied by visualization of oxygen partial pressures in a PEFC-start-up/shut-down simulation. J Power Sources 196(6):3003–3008
131. Su Weng FB, Hsu CY, Chen YM (2006) Studies on flooding in PEM fuel cell cathode channels. Int J Hydrogen Energy 31(8):1031–1039
132. Ous T, Arcoumanis C (2009) Visualisation of water accumulation in the flow channels of PEMFC under various operating conditions. J Power Sources 187(1):182–189
133. Weinmueller C, Tautschnig G, Hotz N, Poulikakos D (2010) A flexible direct methanol micro-fuel cell based on a metalized, photosensitive polymer film. J Power Sources 195 (12):3849–3857
134. Jiao K, Park JW, Li X (2010) Experimental investigations on liquid water removal from the gas diffusion layer by reactant flow in a PEM fuel cell. Appl Energy 87(9):2770–2777
135. Zhan Z, Wang C, Fu W, Pan M (2012) Visualization of water transport in a transparent PEMFC. Int J Hydrogen Energy 37(1):1094–1105
136. Oliveira VB, Rangel CM, Pinto AMFR (2010) Effect of anode and cathode flow field design on the performance of a direct methanol fuel cell. Chem Eng J 157(1):174–180
137. Iranzo A, Muñoz M, Lòpez E, Pino J, Rosa F (2010) Experimental fuel cell performance analysis under different operating conditions and bipolar plate designs. Int J Hydrogen Energy 35(20):11437–11447
138. Ni HJ, Zhang CJ, Wang XX, Ma SY, Liao P (2010) Performance of special-shaped direct methanol fuel cell with sol–gel flux phase. J Fuel Chem Techno 38(5):604–609
139. Kumar A, Reddy RG (2006) Effect of gas flow-field design in the bipolar/end plates on the steady and transient state performance of polymer electrolyte membrane fuel cells. J Power Sources 155(2):264–271
140. Chen YS, Peng H (2011) Predicting current density distribution of proton exchange membrane fuel cells with different flow field designs. J Power Sources 196(4):1992–2004
141. Yang H, Zhao TS (2005) Effect of anode flow field design on the performance of liquid feed direct methanol fuel cells. Electrochim Acta 50(16):3243–3252
142. Hsieh SS, Her BS (2007) Heat transfer and pressure drop in serpentine μDMFC flow channels. Int J Heat Mass Transfer 50(25):5323–5327
143. Lu Y, Reddy RG (2011) Effect of flow fields on the performance of micro-direct methanol fuel cells. Int J Hydrogen Energy 36(1):822–829
144. Dokkar B, Settou NE, Imine O, Saifi N, Negrou B, Nemouchi Z (2011) Simulation of species transport and water management in PEM fuel cells. Int J Hydrogen Energy 36(6): 4220–4227
145. Hsuen HK, Yin KM (2011) A pseudo-phase-equilibrium approach for the calculation of liquid water saturation in the cathode gas diffuser of proton-exchange-membrane fuel cells. Int J Hydrogen Energy 36(9):5487–5499
146. Berning T, Odgaard M, Kær SK (2010) A study of multi-phase flow through the cathode side of an interdigitated flow field using a multi-fluid model. J Power Sources 195(15):4842–4852
147. Le D, Zhou B (2010) A numerical investigation on multi-phase transport phenomena in a proton exchange membrane fuel cell stack. J Power Sources 195(1):5278–5291
148. Hao L, Cheng P (2009) Lattice Boltzmann simulations of liquid droplet dynamic behavior on a hydrophobic surface of a gas flow channel. J Power Sources 190(2):435–446
149. Basu S (2011) A generalized multiphase mixture (M2) model for PEFC flow field design. Int J Hydrogen Energy 36(16):9855–9863
150. Anderson R, Wilkinson DP, Bi X, Zhang L (2010) Two-phase flow pressure drop hysteresis in parallel channels of a proton exchange membrane fuel cell. J Power Sources 195(13): 4168–4176
151. Anderson R, Wilkinson DP, Bi X, Zhang L (2011) Two-phase flow pressure drop hysteresis in an operating proton exchange membrane fuel cell. J Power Sources 196(19):8031–8040
152. Xu C, Faghri A (2010) Water transport characteristics in a passive liquid-feed DMFC. Int J Heat Mass Transfer 53(9):1951–1966

153. Ko J, Chippar P, Ju H (2010) A one-dimensional, two-phase model for direct methanol fuel cells—Part I: model development and parametric study. Energy 35(5):2149–2159
154. Zhou Y, Lin G, Shin AJ, Hu SJ (2009) Multiphysics modeling of assembly pressure effects on proton exchange membrane fuel cell performance. J Fuel Cell Sci Tech 6(1–7)
155. Zhou P, Wu CW, Ma GJ (2007) Influence of clamping force on the performance of PEMFCs. J Power Sources 163(2):874–881
156. Akiki T, Charon W, Iltchev MC, Accary G, Kouta R (2010) Influence of local porosity and local permeability on the performances of a polymer electrolyte membrane fuel cell. J Power Sources 195(16):5258–5268
157. Um S, Wang CY (2004) Three-dimensional analysis of transport and electrochemical reactions in polymer electrolyte fuel cells. J Power Sources 125(1):40–51
158. Chippar P, Oh K, Kim WG, Ju HC (2014) Numerical analysis of effects of gas crossover through membrane pinholes in high-temperature proton exchange membrane fuel cells. Int J Hydrogen Energy 39(6):2863–2871
159. Kwon J, Kang MS et al (2011) Development of flow field design of polymer electrolyte membrane fuel cell using in-situ impedance spectroscopy. Int J Hydrogen Energy 36(16): 9799–9804
160. Park YC, Peck DH et al (2011) Operating characteristics and performance stability of 5 W class direct methanol fuel cell stacks with different cathode flow patterns. Int J Hydrogen Energy 36(2):1853–1861
161. Wang SJ, Huo WW, Zou ZQ, Qia YJ, Yang H (2011) Computational simulation and experimental evaluation on anodic flow field structures of micro direct methanol fuel cells. Appl Therm Eng 31(14):2877–2884
162. Iranzo A, Muñoz M, Pino J, Rosa F (2011) Update on numerical model for the performance prediction of a PEM Fuel Cell. Int J Hydrogen Energy 36(15):9123–9127
163. Xu Z, Qi Z, He C, Kaufman A (2006) Combined activation methods for proton-exchange membrane fuel cells. J Power Sources 156(2):315–320
164. Choi KS, Kim BG, Park K, Kim HM (2012) Flow control of under-rib convection enhancing the performance of proton exchange membrane fuel cell. Comput Fluids 69:81–92
165. Vinh ND, Kim HM et al (2015) Dynamic simulations of under-rib convection-driven flow-field configurations and comparison with experiment in polymer electrolyte membrane fuel cells. J Power Sources 293:447–457
166. Radhakrishnan V, Haridoss P (2011) Effect of GDL compression on pressure drop and pressure distribution in PEMFC flow field. Int J Hydrogen Energy 36(12):14823–14828
167. Hutzenlaub T, Paust N, Zengerle R, Ziegler C (2011) The effect of wetting properties on bubble dynamics and fuel distribution in the flow field of direct methanol fuel cells. J Power Sources 196(19):8048–8056